Analysis of Allosteric Communication Pathways in Class I Glutamine Amidotransferases

Dissertation

zur Erlangung des Doktorgrades der Naturwissenschaften (Dr. rer. nat.) der Fakultät für Biologie und vorklinische Medizin der Universität Regensburg

vorgelegt von
Florian Semmelmann
aus Deggendorf

Juli 2019

Das Promotionsgesuch wurde eingereicht am: 12.07.2019

Die Arbeit wurde angeleitet von: Prof. Dr. Reinhard Sterner

Unterschrift: .....

Florian Semmelmann

Die vorliegende Arbeit wurde im Zeitraum von Oktober 2015 bis Juli 2019 am Lehrstuhl Biochemie II des Institutes für Biophysik und Physikalische Biochemie der Fakultät für Biologie und Vorklinische Medizin der Universität Regensburg unter Leitung von Prof. Dr. Reinhard Sterner angefertigt.

Diese Arbeit wurde vom 01.01.2016 bis zum 31.12.2018 durch ein Promotionsstipendium der *Konrad-Adenauer-Stiftung* gefördert.

Konrad
Adenauer
Stiftung

Abstract

Class I glutamine amidotransferases (GATases) represent a ubiquitous family of enzymes that catalyze the incorporation of ammonia within various metabolic pathways. GATases are heteromeric enzyme complexes consisting of at least one pair of glutaminase and synthase subunits in various oligomeric associations. The activities of the glutaminase and synthase subunits are allosterically coupled in most class I GATases in a way that the presence of substrate at the synthase subunit stimulates glutamine hydrolysis at the glutaminase active site. The structural basis of allosteric communication between both subunits is, however, not well understood.

The first part of this thesis focuses on the molecular basis of allosteric coupling in 4-amino-4-deoxychorismate synthase (ADCS), an important but hitherto sparsely characterized member of class I GATases. Using ancestral sequence reconstruction, we generated a thermostable glutaminase subunit, *anc*2PabA, solved its crystal structure by molecular replacement and used it to compute for the first time a reliable model of the *E. coli* ADCS complex. Alanine scanning of conserved residues located between the glutaminase and synthase active sites revealed a network of mainly charged residues that lead to activity-inducing conformational changes at the glutaminase subunit. A central aspartate residue of the synthase subunit that is located at the synthase-glutaminase interface close to the active site of the glutaminase subunit, was identified as key residue for both complex formation and allosteric signaling.

The second part of this thesis describes the bioinformatic search and biochemical characterization of similarly located aspartate residues in the remaining members of class I GATases. The data confirms the important role of the identified aspartate residues for complex formation and allosteric signaling and is integrated toward a unifying allosteric core mechanism for class I GATases.

References of Published Manuscripts

This thesis is composed of the following manuscripts:

A Adapted with permission from "**Semmelmann, F.**, Straub, K., Nazet, J., Rajendran, C., Merkl, R. & Sterner, R. (2019). Mapping the Allosteric Communication Network of Aminodeoxychorismate Synthase. *Journal of Molecular Biology*, 431(15), 2718-2728. Copyright (2019) Elsevier."

B Adapted with permission from "**Semmelmann, F.**, Hupfeld, E., Heizinger, L., Merkl, R., & Sterner. R. (2019). A Fold-Independent Interface Residue is Crucial for Complex Formation and Allosteric Signaling in Class I Glutamine Amidotransferases. *Biochemistry*, 58(22), 2584-2588. Copyright (2019) American Chemical Society."

In the course of this work, I contributed to further publications that are not part of this thesis:

C **Semmelmann, F.**, Kabeya, N., Malcicka, M., Bruckmann, A., Broschwitz, B., Straub, K., Merkl, R., Monroig, O., Sterner, R., Ruther, J. & Ellers, J. (2019). Functional characterisation of two Δ12-desaturases demonstrates targeted production of linoleic acid as pheromone precursor in *Nasonia*. *Journal of Experimental Biology*, 222(10), jeb201038.

D **Semmelmann, F.**, Hofferberth, J., Ruther, J. & Sterner, R. (2019). Mapping key amino acid residues for the epimerase efficiency and stereospecificity of the sex pheromone biosynthetic short-chain dehydrogenases/reductases of *Nasonia*. *Scientific Reports*, 9(1), 330.

E Rohweder, B., **Semmelmann, F.**, Endres, C. & Sterner, R. (2018). Standardized cloning vectors for protein production and generation of large gene libraries in *Escherichia coli*. *BioTechniques*, 64(1), 24-26.

Personal Contributions

Publication A

The research was designed by myself and Reinhard Sterner. Kristina Straub performed ancestral sequence reconstruction and Julian Nazet performed homology modeling. Chitra Rajendran collected diffraction data. All other experiments were performed by myself. The publication was written by myself, Rainer Merkl, and Reinhard Sterner with contributions from Kristina Straub and Julian Nazet.

Publication B

The research was designed by myself and Reinhard Sterner. Leonhard Heizinger and myself provided computational tools and scripts. Enrico Hupfeld contributed data on the imidazole glycerole phosophate synthase. All other experiments were performed by myself. The publication was written by myself, Rainer Merkl, and Reinhard Sterner with contributions from Leonhard Heizinger and Enrico Hupfeld.

Contents

List of Figures

List of Tables

Chapter 1

General Introduction

> "It is certain that all bodies whatsoever, though they have no sense, yet they have perception; for when one body is applied to another, there is a kind of election to embrace that which is agreeable, and to exclude or expel that which is ingrate; and whether the body be alterant or altered, evermore a perception precedeth operation; for else all bodies would be like one to another."
>
> *Francis Bacon* (about 1620)

1.1 A Short Introduction to Allostery

Allostery is the regulatory phenomenon by which proteins convey the effect of ligand binding at one site to a distant functional site (Motlagh et al., 2014). The term allostery (from greek *allos* for "other" and *stereos* for "solid") was first articulated in the 1960s by Monod, Changeux, and Jacob in their pioneer work on "Allosteric Proteins and Cellular Control Systems" (Monod et al., 1963). Ever since, allostery has elicited much attention both because of its exceptional physiological importance and the challenge its biophysical interpretation offered (Monod et al., 1965). For the latter, the advent of protein X-Ray crystallography techniques and especially the determination of the hemoglobin crystal structure (Figure 1.1) (Perutz et al., 1960), the prime example of allosteric proteins, preluded the era of the *static view of allostery*, which was to become the reigning paradigm to describe allostery for decades thereafter. This interpretation of allostery was centered around crystal structures of apo and holo forms of proteins and thus delivered a qualitative view of allostery that was greatly influenced by static structural images of end-point protein structures (i.e. unbound or tensed (T) vs. bound or relaxed (R) state). In order to describe the observed biochemical and crystallographic data, the (i) concerted model (Monod et al., 1965) and the (ii) sequential model (Koshland Jr et al., 1966) were developed. Whereas the concerted model interprets the coupling of subunits as absolute, the sequential model interprets the coupling between ligand binding and conformational change of an individual subunit as absolute. More recently, however, it has been postulated that a functional state is not necessarily linked to either the tensed or relaxed state of a protein. Rather, changes in the

conformational heterogeneity (local unfolding, intrinsic disorder, and conformational dynamics) of proteins seem to contribute to allosteric transitions (Hilser, 2010). This view of allostery is now commonly referred to as the *ensemble view of allostery*. Despite its importance, the physical basis of allosteric transitions has only been well understood for very few enzyme systems (Lisi and Loria, 2016) and a prerequisite for detailed analysis of allosteric transitions are structural data to interpret the observed allosteric regulation patterns. Studies on model systems are thus pivotal to further decipher the molecular basis of allosteric transitions and to eventually unravel potential universal patterns.

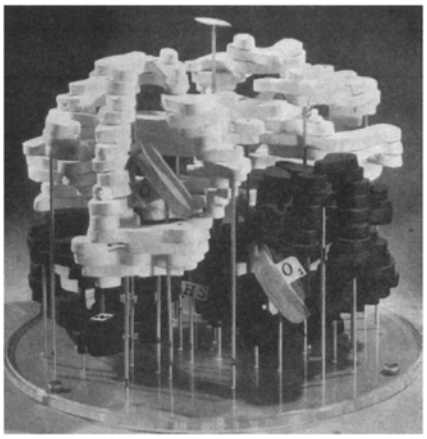

Figure 1.1: Model of hemoglobin. The haem groups are indicated as gray disks. The four protomers are shown in white and black. Figure reprinted by permission from Springer Nature: Nature (Perutz et al., 1960), copyright 1960.

1.2 The Family of Glutamine Amidotransferases

The heteromeric enzyme complexes of the family of glutamine amidotransferases (GATases) are well-established model systems to study the molecular basis of allosteric communication (Mouilleron et al., 2011; List et al., 2012b; Lisi et al., 2018; Negre et al., 2018). GATase enzyme complexes consist of at least one pair of glutaminase and synthase domains/subunits that are localized either on the same or on different polypeptide chains. The glutaminase domain/subunit hydrolyzes glutamine to glutamate and nascent ammonia, which is channeled to the synthase domain/subunit active site where it is incorporated into specific acceptor substrates (Huang et al., 2001) (Figure 1.2 A). GATases catalyze the incorporation of ammonia into a variety of acceptor substrates within different metabolic pathways (Figure 1.2 B) (Zalkin and Smith, 1998). Whereas the synthase subunits belong to several, structurally unrelated protein families, the glutaminase domains/subunits can be categorized into two classes according to their fold and active site composition. Class I GATases comprise enzyme complexes whose glutaminase subunits possess a catalytic Cys-His-Glu triad and an α/β hydrolase fold (Ollis et al., 1992). This class consists of the enzyme complexes imidazole glycerol phosphate synthase (ImGPS) (Chaud-

huri et al., 2003; Douangamath et al., 2002), anthranilate synthase (AS) (Knöchel et al., 1999; Morollo and Eck, 2001; Spraggon et al., 2001), 4-amino-4-deoxychorismate synthase (ADCS) (Parsons et al., 2002; Bera et al., 2012), carbamoylphosphate synthetase (CPS) (Thoden et al., 1997), guanosin-5‘-monophosphate synthase (GMPS) (Tesmer et al., 1996), formylglycinamide ribonucleotide synthetase (FGARS) (Anand et al., 2004), cytidin 5’-triphosphate synthetase (CTPS) (Goto et al., 2004), 2-amino-2-deoxyisochorismate synthase (PhzE) (Li et al., 2011) and pyridoxalphosphate synthase (PS) (Strohmeier et al., 2006; Raschle et al., 2005; Zein et al., 2006; Bauer et al., 2004). Class II GATases, in contrast, comprise enzyme complexes whose glutaminase subunits possess a N-terminal catalytic cysteine residue and a Ntn-hydrolase fold. This class consists of the enzyme complexes glutamine phosphoribosylpyrophosphate amidotransferase (Kim et al., 1996), glucosamin-6-phosphate-synthase (Mouilleron and Golinelli-Pimpaneau, 2007), asparagine- and glutamate synthase (Nakatsu et al., 1998; Binda et al., 2000). To prevent the unproductive hydrolysis of glutamine, GATases evolved sophisticated allosteric coupling mechanisms between their synthase and glutaminase subunits. These coupling mechanisms assure that ammonia is only efficiently generated at the glutaminase subunit when concomitantly there is acceptor substrate bound at the synthase subunit active site (Mareya and Raushel, 1994; Bera et al., 1999; Beismann-Driemeyer and Sterner, 2001). While conformational changes underlying the allosteric coupling of synthase and glutaminase subunits have been well characterized for glucosamin-6-phosphate-synthase, a member of class II GATases, less is known for class I GATases.

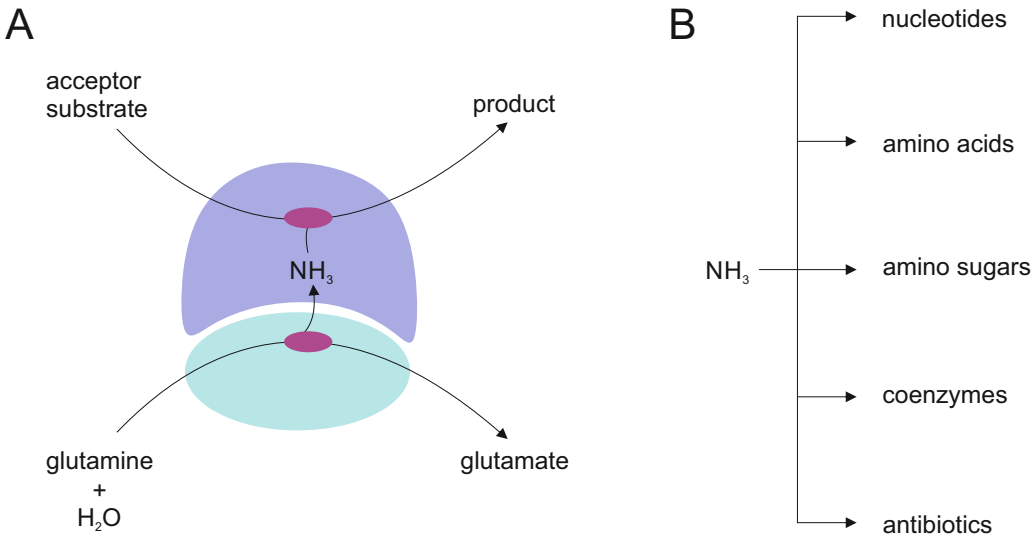

Figure 1.2: Reaction catalyzed by GATases and metabolic fates of ammonia. (A) The glutaminase subunit is depicted in cyan, the synthase subunit in blue. Active sites are indicated in purple. Glutamine is hydrolyzed at the glutaminase active site to glutamate and ammonia (NH_3), which is channeled through a tunnel to the active site of the synthase where it is incorporated into the synthase-specific acceptor substrates. The products of this reaction are either released from the synthase subunit acitve site or undergo additional chemical modifications. (B) The products of the GATase reaction are precursors for the biosynthesis of various different metabolites.

1.2.1 Structural Diversity Within the Synthase Subunits of Class I GATases

It is still unclear, however, if the allosteric regulation mechanisms of class I GATases evolved independently for the individual members of this enzyme family or if there are commonalities between them. Whereas the similarities in structure and active site composition in the glutaminase subunits indicate a potential uniform allosteric regulation mechanism, the observed structural diversity within the synthase subunits does not support this notion. The latter ranges from $(\beta/\alpha)_8$-barrel folds (ImGPS, PS) to 4-layer sandwich-fold (AS, ADCS, and PhzE) (Figure 1.3 blue). Additionally, the different oligomeric states observed for these enzymes further complicate the identification of commonalities in allosteric regulation. These range from hetero-dimeric (ImGPS)(Douangamath et al. 2002), intertwined homo-dimeric fusions of glutaminase and synthase domain (PhzE) (Strohmeier et al., 2006), hetero-tetrameric (AS) (Knöchel et al., 1999), to dodecamers of hetero-dimeric (PS) (Zein et al., 2006; Strohmeier et al., 2006) associations (Figure 1.3).

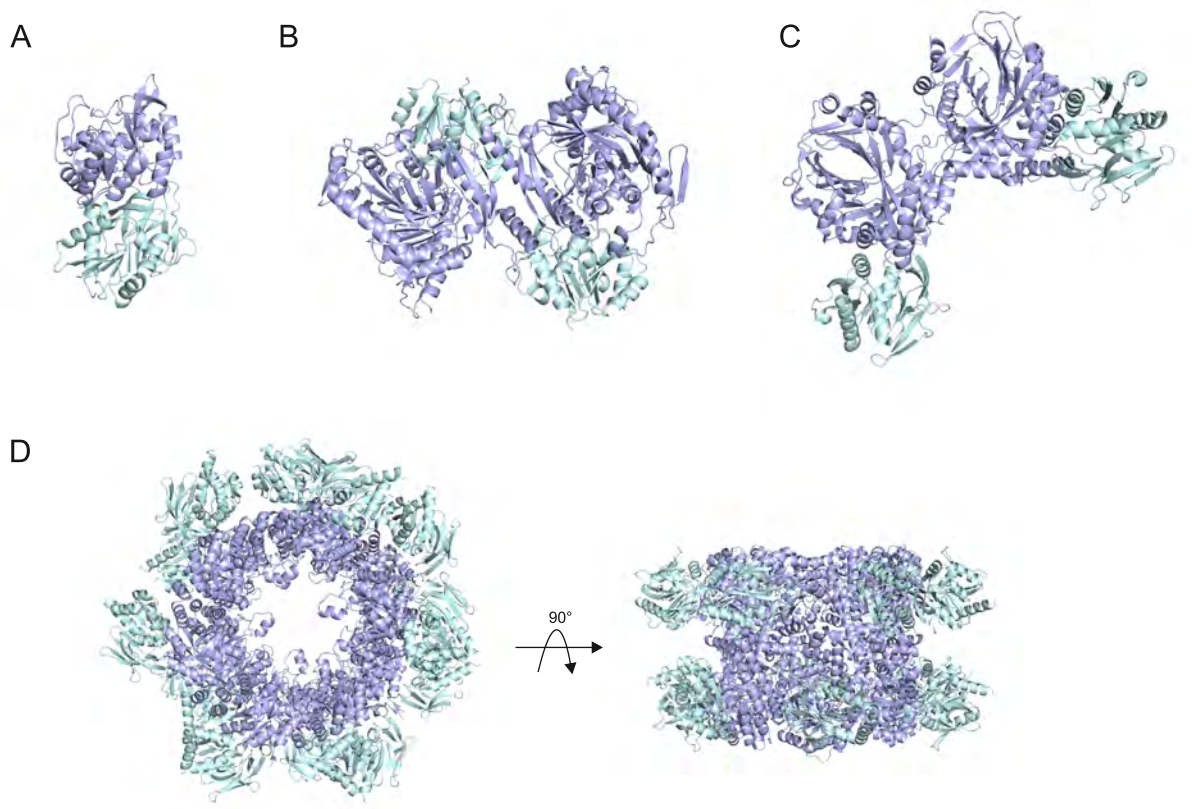

Figure 1.3: Structural diversity observed in class I glutamine amidotransferases. (A) Imidazole glycerol phosphate synthase from *Thermotoga maritima* (PDB ID: 1GPW) (B) Anthranilate synthase from *Salmonella typhimurium* (PDB ID: 1I1Q) (C) 2-amino-2-deoxyisochorismate synthase from *Burkholderi lata* (PDB ID: 3R74) (D) Pyridoxalphosphate synthase from *Bacillus subtilis* (PDB ID: 2NV2). Glutaminase subunits/domains are depicted in cyan and synthase subunits/domains are depicted in blue.

Strikingly, for all members of class I GATases except for 4-amino-4-deoxychorismate synthase (ADCS) there are high-resolution crystal structures of either the complexes of synthase and glutaminase subunits and/or of the autonomous subunits available. For ADCS, however, there are only two autonomous structures of its synthase subunit described in the literature. Studies on the allosteric mechanism underlying glutaminase activation in ADCS have thus been hampered by the absence of an autonomous glutaminase subunit structure for ADCS.

1.2.2 Structural and Functional Insights into 4-Amino-4-Deoxychorismate Synthase

ADCS catalyzes the committed step in the biosynthesis of folate by incorporating ammonia into chorismate. Due to its sole appearance in bacteria, fungi, and plants, the enzyme has received significant interest as potential target of antimicrobial drugs (Davies et al., 1994; Bulloch et al., 2004). Drug development has halted though, most presumably due to missing structural information on the glutaminase-synthase complex. To date, only two crystal structures of the autonomous PabB synthase subunits from *Escherichia coli* (Parsons et al., 2002) and *Stenotrophomonas maltophilia* (Bera et al., 2012) have been described in literature (Figure 1.4).

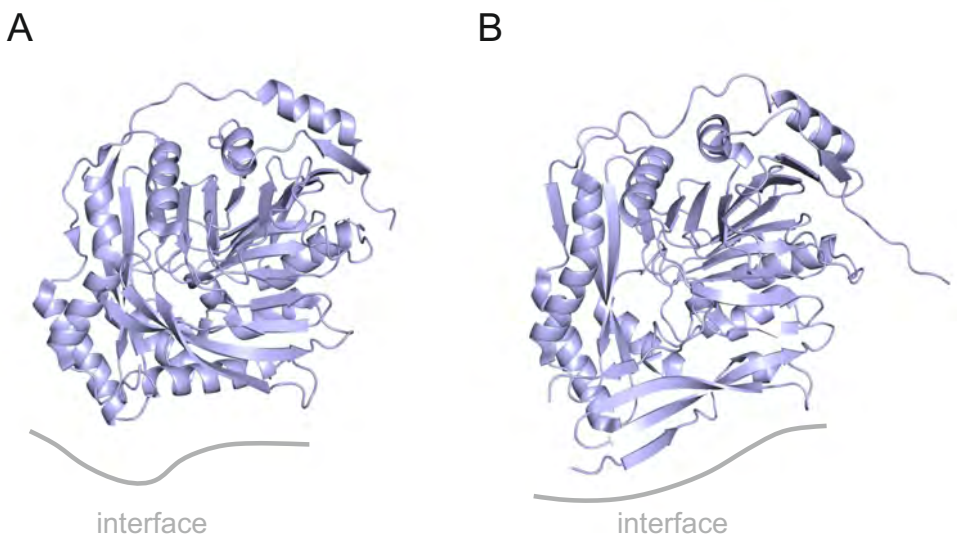

Figure 1.4: Crystal structures of autonomous PabB structures from (A) *E. coli* (PDB ID: 1K0E) and (B) *S. maltophilia* (PDB ID: 4GRH). The synthase subunits are depicted in blue, the potential (partially disordered) PabA binding sites are indicated as gray lines.

Both structures display a complex 4-layer sandwich fold similar to the synthase subunits of the homologous anthranilate synthases (Knöchel et al., 1999; Morollo and Eck, 2001). Even though both structures show significant disorder at the proposed PabA binding site (indicated in gray in Figure 1.4), they still allowed valuable insights into the reaction mechanism underlying ammonia incorporation into chorismate in these enzymes (He et al., 2004; He and Toney, 2006; Viswanathan et al., 1995).

Mechanistically, PabB enzymes can be categorized into either the "PI**K**GT"- or "PI**A**GT"- motif group. According to the unifying core mechanism for chorismate utilizing enzymes (He et al., 2004), a central lysine residue (K274 in the enzyme from *E. coli*) of the "PI**K**GT"-motif covalently binds to C2 of chorismate to initiate the reaction. The covalent attack of lysine leads to elimination of the hydroxyl-group at C4. The subsequent substitution of ammonia at C4 leads to an inversion of the stereochemistry at C4 and concomitant displacement of lysine ends the catalytic cycle (Figure 1.5 A). Enzymes of the "PI**A**GT" group utilize two equivalents of ammonia to generate 4-amino-4-deoxychorismate from chorismate. The first equivalent of ammonia attacks at C2 of chorismate with concomitant elimination of hydroxyl-group at C4 to yield 2-amino-2-deoxyisochorismate as intermediate. The subsequent addition of ammonia at C4 leads to a displacement of ammonia at C2 to end the catalytic cycle (Bera et al., 2012; Schadt et al., 2009) (Figure 1.5 B).

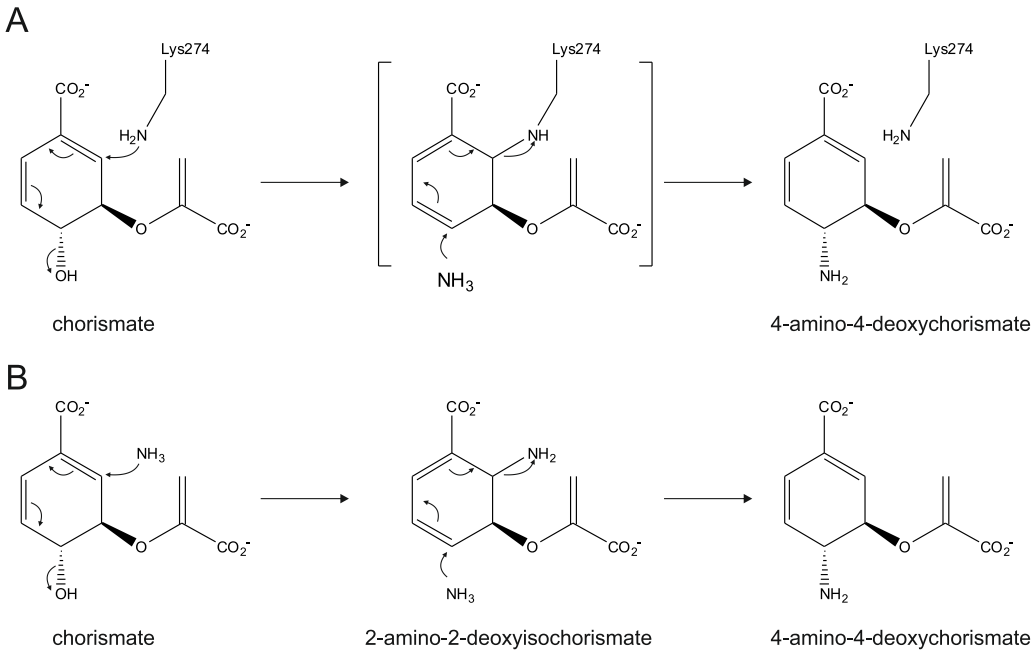

Figure 1.5: Proposed reaction mechanisms of PabB. (A) "PI**K**GT"-motif group: The catalytic cycle is initiated by the attack of a highly conserved lysine residues (K274 from the enzyme of *E. coli*) at C2 of chorismate resulting in displacement of the hydroxyl-group at C4. In a second SN2 reaction, ammonia attacks at C4 and lysine (K274) is displaced and 4-amino-4-deoxychorismate released from the active site. (B) "PI**A**GT"-motif group: The catalytic cycle is initiated by the attack of one equivalent of ammonia at C2 of chorismate resulting in displacement of the hydroxyl-group at C4 to yield 2-amino-2-deoxyisochorismate as intermediate. A second equivalent of ammonia subsequently attacks at C4 and ammonia at C2 is displaced and 4-amino-4-deoxychorismate released from the active site.

1.3 Aim and Scope of This Work

The aim of this work was to contribute to the understanding of the molecular basis of allosteric coupling in class I GATases. To this end, we sought to provide the missing structural information on the ADCS glutaminase subunit PabA to allow computation of a reliable homology model of the ADCS complex structure. To identify residues that are involved in allosteric communication, individual conserved amino acid side chains that are located between the PabA and the PabB active site should be replaced by alanine and their contribution to allosteric signaling studied by steady-state enzyme kinetics. Furthermore, we sought to consolidate these and previous findings on other class I enzyme systems to develop a generalized hypothesis of allosteric regulation.

1.4 Guide to the Following Chapters

The two following chapters are composed of the two first-author publications (A-B) that constitute this thesis.

The publication **Mapping the Allosteric Communication Network of Aminodeoxychorismate Synthase** describes an in-depth analysis of allosteric coupling in 4-amino-4-deoxychorismate synthase (ADCS). Ancestral sequence reconstruction was used to derive a thermostable PabA glutaminase subunit that was crystallized and its structure solved by molecular replacement. This PabA structure was then used to compute a reliable homology model of the *E. coli* PabA-PabB complex. Alanine-scanning at conserved residues located between the PabA and PabB active sites revealed four branches of an allosteric communication pathway that lead to activity-inducing conformational changes at the PabA active site as a consequence of chorismate binding at the PabB active site. Three conserved interaction hot-spot residues in the glutaminase-synthase interface were identified, one of which, a conserved aspartate-residue of the ADCS synthase subunit was identified as key residue for both complex formation and allosteric signaling.

The publication **A Fold-Independent Interface Residue is Crucial for Complex Formation and Allosteric Signaling in Class I Glutamine Amidotransferases** corroborates the dual role of the conserved aspartate residue discovered in ADCS. Computational screening of the Protein Data Bank revealed the presence of similarly located aspartate residues in the synthase subunits of five class I glutamine amidotransferases with different folds/oligomeric states. Mutational analysis of these aspartate residues in four different class I GATase enzyme systems shows the critical role of this residue in complex formation (three out of four cases) and allosteric signaling (all four cases).

Chapter 2

Mapping the Allosteric Communication Network of Aminodeoxychorismate Synthase

2.1 Abstract

Allosteric communication between different subunits in metabolic enzyme complexes is of utmost physiological importance but only understood for few systems. We analyzed the structural basis of allostery in aminodeoxychorismate synthase (ADCS), which is a member of the family of glutamine amidotransferases and catalyzes the committed step of the folate biosynthetic pathway. ADCS consists of the synthase subunit PabB and the glutaminase subunit PabA, which is allosterically stimulated by the presence of the PabB substrate chorismate. We first solved the crystal structure of a PabA subunit at 1.9-Å resolution. Based on this structure and the known structure of PabB, we computed an atomic model for the ADCS complex. We then used alanine scanning to test the functional role of 59 conserved residues located between the active sites of PabB and PabA. Steady-state kinetic characterization revealed four branches of a conserved network of mainly charged residues that propagate the signal from chorismate at the PabB active site to the PabA active site. The branches eventually lead to activity-inducing transformations at (i) the oxyanion hole motif, (ii) the catalytic Cys-His-Glu triad, and (iii) glutamine binding residues at the PabA active site. We compare our findings with previously postulated activation mechanisms of different glutamine amidotransferases and propose a unifying regulation mechanism for this ubiquitous family of enzymes.

2.2 Introduction

Allostery is an integral property of enzymes that allows for the regulation of activity in response to the physiological needs of a cell (Monod et al., 1965). Thereby, ligand binding to an *allosteric site* induces signal propagation via protein backbone or amino acid side-chain movements to affect function at a distant *active site*. Understanding the molecular details of signal propagation between the two sites is an important biochemical challenge both for applied and basic

protein biochemistry. In applied research, molecular details of allosteric communication have the potential to reveal binding sites for novel drugs that perturb signal propagation (Chen et al., 2016; Monaghan et al., 2012; Fang et al., 2012; Selvy et al., 2011; Kenakin and Miller, 2010; Rivalta et al., 2016; Goto et al., 2004). In basic research, the identification of signal propagation pathways is crucial for unraveling universal patterns of the underlying dynamic adaptability of enzymes (Gunasekaran et al., 2004).

A paradigm for studying the molecular basis of allosteric communication are glutamine amidotransferases (GATases). GATases form a large enzyme family, whose members are responsible for the incorporation of nitrogen within numerous metabolic pathways (Mouilleron and Golinelli-Pimpaneau, 2007; Raushel et al., 1999; Zalkin and Smith, 1998). Most GATases are bi-enzyme complexes, consisting of a synthase and a glutaminase subunit, whose activities are mutually coupled: Substrate binding to the synthase subunit allosterically induces glutamine hydrolysis to glutamate and ammonia at the glutaminase subunit. Nascent ammonia is then transported through an intermolecular channel to the active site of the synthase subunit, where it reacts with the "waiting" substrate to specific reaction products. While the synthase subunits of the various GATases are structurally diverse, the glutaminases can be categorized into two classes according to their fold and active site composition: class I glutaminases possess a α/β-hydrolase fold and a catalytic Cys–His–Glu triad (Ollis et al., 1992); in contrast, class II glutaminases possess an Ntn-hydrolase fold and a catalytic N-terminal Cys (Brannigan et al., 1995). Whereas the structural basis of allosteric communication is understood to a certain degree for class II GATases (Mouilleron et al., 2011), even a basic understanding of the allosteric communication pathways within class I GATases is still lacking.

An interesting member of class I GATases is aminodeoxychorismate synthase (ADCS), which consists of the glutaminase subunit PabA and the synthase subunit PabB. It catalyzes the committed step in the biosynthesis of folate by incorporating nitrogen into chorismate to yield 4-amino-4-deoxychorismate (Figure 2.1).

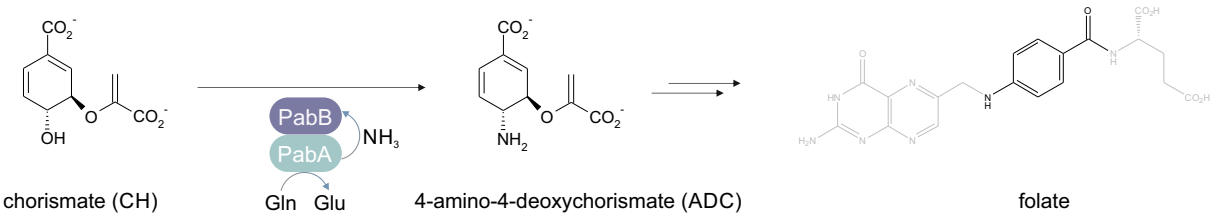

Figure 2.1: Reaction catalyzed by ADCS. The glutaminase subunit PabA hydrolyzes glutamine (Gln) to glutamate (Glu) and nascent ammonia (NH_3), which is channeled to the active site of the synthase subunit PabB where it reacts with chorismate (CH) to form 4-amino-4-deoxychorismate (ADC). ADC is a precursor in the biosynthesis of folate (shown in gray except the part of the molecule that stems from ADC).

Glutamine hydrolysis by PabA is activated upon complex formation with PabB and further allosterically stimulated by chorismate binding to the synthase active site. Thus, the active site of PabB acts as an allosteric site that, upon binding of its substrate, stimulates activity at the

PabA active site. In spite of the identification of key catalytic amino acid residues in PabA and PabB (Rayl et al., 1996; Roux and Walsh, 1992), the availability of two PabB crystal structures (Parsons et al., 2002; Bera et al., 2012), and a basic understanding of the chemical reaction mechanisms for PabA and PabB (He et al., 2004; Culbertson et al., 2015), the structural basis for allosteric communication in ADCS still awaits clarification.
Here, we addressed allostery in ADCS by a combination of experimental and computational approaches. We first solved the structure of a stable PabA subunit at high resolution. Together with the known structure of a PabB subunit, we then generated a homology model of the ADCS complex and performed a comprehensive alanine-scanning approach at conserved residues of both subunits. The results allowed us to define the allosteric communication pathway within ADCS. Specifically, we identified a conserved network of mainly hydrogen-bonded residues that propagates the signal from the *allosteric site* in PabB to the *active site* in PabA.

2.3 Results

2.3.1 Crystal Structure Analysis of PabA and Homology Modeling of ADCS

In order to map the allosteric communication network of ADCS, we first set out to provide the missing structural information for PabA. Despite extensive efforts, we were not able to crystallize modern PabA enzymes (from *E. coli*, *Bacillus subtilis*, *Serratia marcescens*, and *Pseudomonas putida*) (Plach et al., 2017). Ancestral sequence reconstruction often yields thermostable proteins (Wheeler et al., 2016), which have a higher tendency to crystallize than their thermolabile homologs. Therefore, we reconstructed ancestral PabA sequences based on the sequences of 59 recent homologs from Firmicutes, Fusobacteria, Proteobacteria, and Halobacteriales (Figure 2.7). The genes encoding the three most ancient bacterial predecessors (*anc*1–3PabA) were expressed in *E. coli*, and the recombinant proteins were purified and biochemically characterized. Interestingly, all three enzymes were more thermostable than modern PabA proteins (Tables 2.1, 2.2, 2.3), formed stable complexes with modern PabB subunits (Table 2.4), and were stimulated by them (Table 2.5). From these ancestral PabA enzymes, we were able to only crystallize *anc*2PabA and solved its structure by molecular replacement using the homologous class I glutaminase subunit from *Sulfolobus solfataricus* anthranilate synthase (AS) (PDB ID: 1QDL; sequence identity: 51%, sequence similarity: 66%) as template (Table 2.6). The structure of *anc*2PabA (PDB ID: 6QUR) possesses the same α/β-hydrolase fold as the glutaminase subunits of the GATases AS and imidazole glycerol phosphate synthase (ImGPS) (Figure 2.2) (Morollo and Eck, 2001; Knöchel et al., 1999; Douangamath et al., 2002).

The catalytic triad consisting of *a*C79, *a*H168, and *a*E170 is located at the solvent-accessible active site (*a* connotes residues in PabA, and *b* connotes residues in PabB). Surprisingly, the crystal structure of *anc*2PabA features a disulfide bond between the catalytic *a*C79 residue

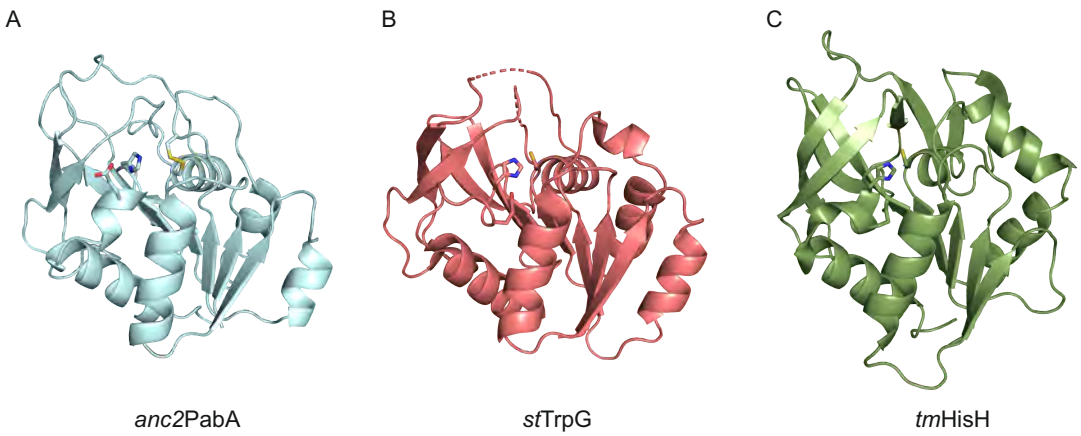

Figure 2.2: Structural comparison of *anc*2PabA to homologous class I glutaminase subunits. (A) Crystal structure of *anc*2PabA (PDB ID: 6QUR); disulfide bond formed between *a*C54 and *a*C79 and the catalytic Cys–His–Glu triad is shown as sticks. (B) Crystal structure of the glutaminase subunit *st*TrpG from *Salmonella typhimurium* AS (PDB ID: 1I1Q). (C) Crystal structure of the glutaminase subunit *tm*HisH from *T. maritima* ImGPS (PDB ID: 1GPW). Sequence identity between *anc*2PabA and *st*TrpG is 84/198 (42.4%) and sequence similarity is 115/198 (58.1%). Sequence identity between *anc*2PabA and *tm*HisH is 50/231 (21.6%), and sequence similarity is 84/231 (36.4%). The structure of *anc*2PabA superimposes well with those of *st*TrpG and *tm*HisH with all-atom RMSDs of 1.6 Å (*anc*2PabA-*st*TrpG) and 2.9 Å (*anc*2PabA-*tm*HisH), respectively.

and *a*C54, which is located in a loop covering the active site adjacent to a sequence stretch referred to as the *oxyanion hole* motif (*a*P51–*a*G52–*a*P53–*a*C54) (Rivalta et al., 2012). Since our previous crystallization trials with a variety of modern PabA and PabA:PabB complexes failed, we assume that formation of this disulfide bond in *anc*2PabA stabilizes the enzyme and thus ultimately allowed for its crystallization.

Based on the crystal structure of *anc*2PabA, we generated a homology model for the *E. coli* ADCS complex by superimposing the previously solved *ec*PabB structure (PDB ID: 1K0E) and a model of *ec*PabA [that we generated based on the structure of *anc2*PabA (PDB ID: 6QUR)] with the homologous AS complex from *S. solfataricus* (PDB ID: 1QDL) (Table 2.7). To generate the final model of the holo enzyme, we superposed the substrates chorismate and glutamine from the structure of *S. marcescens* AS (PDB ID: 1I7Q) into the active sites of PabB and PabA, respectively. The model was energy minimized within YASARA's "build model" function (Krieger and Vriend, 2014) and further relaxed by molecular dynamics simulations for 100 ns with GROMACS (Berendsen et al., 1995; Lindahl et al., 2001).

2.3.2 Alanine Scanning for the Identification of Residues Involved in Allosteric Signal Propagation

To identify residues in the ADCS complex that propagate the allosteric signal induced by chorismate binding to PabB onto PabA, we individually replaced 59 conserved residues located between both active sites by alanines (wild-type alanines were replaced by valines, respectively)

using site-directed mutagenesis. We expressed the mutated genes in *E. coli*, purified the soluble recombinant enzymes (Table 2.8) and analyzed the effect of each individual mutation on complex formation and activity.

The results of analytical size exclusion chromatography showed that all mutant enzymes except those carrying the exchanges *a*Y127A, *b*D308A, and *b*R311A formed stable ADCS complexes with the corresponding wild-type partner subunit (Figure 2.9 and Table 2.4). These three "interaction hotspot residues" are embedded in an inter-domain hydrogen bonding network that comprises residues *a*Y18, *a*Y127, *a*E170 (backbone), *a*S171, *b*D308, and *b*R311 (Figure 2.8).

For the mutant enzymes that formed stable ADCS complexes with the corresponding wild-type partner subunits, we quantified the extent of allosteric PabA activation by determining the apparent glutamine hydrolysis rate (k_{app}). To this end, we incubated PabA with glutamine at saturating concentrations (20 mM) and monitored its hydrolysis before and after the addition of (i) PabB or (ii) PabB + chorismate (saturating concentrations) for all combinations of wild-type-PabA/mutant-PabB and mutant-PabA/wild-type-PabB. For the wild-type complex, the basal glutaminase activity of 0.004 s^{-1} [k_{app}(PabA)] is elevated upon binding of PabB to 0.21 s^{-1} [k_{app}(PabA + PabB)] and further allosterically stimulated in the presence of chorismate to 0.58 s^{-1} [k_{app}(PabA + PabB + CH)]. Basal glutaminase activity was similar to wild-type for all mutant enzymes, except the one containing the *a*T125A exchange (will be discussed below). In contrast, PabA activation was very sensitive to mutations in both PabA and PabB: 24 out of the 49 assayed mutant enzymes showed a more than 2-fold change in k_{app}(PabA + PabB) or k_{app}(PabA + PabB + CH) values (Table 2.5).

In order to identify residues that contribute to allosteric signaling, we compared the ratio of the apparent rates in the presence and absence of chorismate, which we refer to as *allosteric activation factor*. For the wild-type enzyme, the allosteric activation factor is 2.7 [0.58 s^{-1} (k_{app}(PabA + PabB + CH)]/0.21 s^{-1} (k_{app}(PabA + PabB))]. In order to exclude minor secondary effects that resulted from structural perturbations through the introduction of alanine, we defined residues as involved in allosteric signaling when their allosteric activation factor was below 1.5. Eleven mutants displayed allosteric activation factors of 1.0–1.5 indicating no or impaired allosteric activation. Thirteen mutants showed an allosteric activation factor ≤ 1.0, indicating allosteric deactivation (Figure 2.3 A).

We were interested to test whether the effects of mutations on k_{app} for glutamine hydrolysis are at least partially attributed to an increase in the Michaelis constant for glutamine ($K_M{}^{Gln}$) or entirely due to a decrease of the turnover rate (k_{cat}). For this purpose, we followed the glutamine-dependent conversion of chorismate (CH) to aminodeoxychorismate (ADC) for the different ADCS complexes (Table 2.9). The results demonstrated that complexes containing mutant enzymes with the exchanges *a*D6A, *a*Y8A, *a*R30A, *a*R126A, *a*H128A, *a*S129A, *a*L130A, *a*Q166A, *a*I172A *b*E119A, and *b*G207A showed drastically elevated $K_M{}^{Gln}$ values, which might contribute to the observed decreases in k_{app}. The complexes containing the other mutant enzymes showed only minor effects with respect to $K_M{}^{Gln}$, proving that the observed changes in

k_{app} are entirely caused by changes in k_{cat}. Interestingly, we also identified residues involved in ammonia channeling from the active site of PabA to the active site of PabB: Whereas in ADCS complexes containing mutant enzymes with the *a*D9A, *a*H101A, *a*R126A, *a*L130A, *b*D208A, *b*L309A, and *b*G369A exchanges, glutaminase activity was readily stimulated (Figure 2.3 A), no measurable or very low turnover was observed when the ADCS reaction was followed (Table 2.9). The unproductive loss of ammonia in these mutants indicates that the respective wild-type amino acids are involved in ammonia tunnel formation between active sites.

2.3.3 Identification of Four Branches of a Conserved Allosteric Communication Network

We subsequently mapped the 24 allosterically important residues on the model of *E. coli* ADCS and deduced the most plausible pathways for signal propagation between the two active sites. To this end, we drew connecting edges between allosteric residues when either (i) their side chains were in direct van der Waals or hydrogen-bonding contact or (ii) the residues were connected via the protein backbone (Figure 2.3 B).

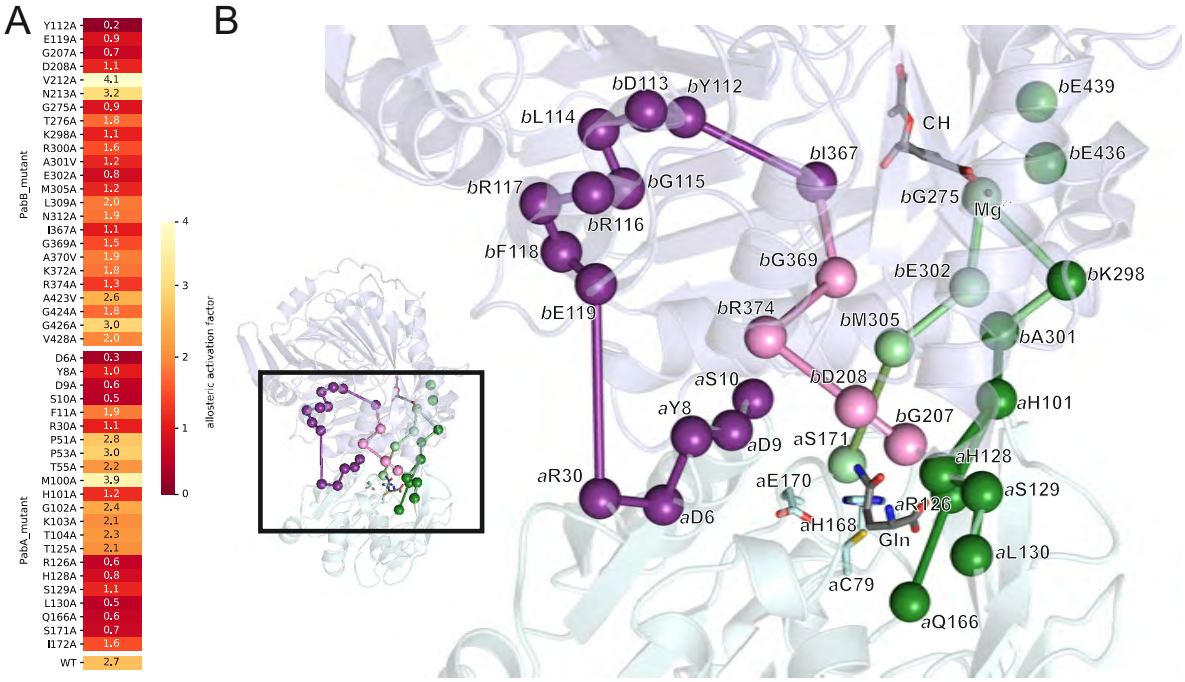

Figure 2.3: Allosteric residues in ADCS. (A) Heat map indicating the ratio of the apparent glutaminase rates in the presence and absence of chorismate (k_{app}(PabA + PabB + CH)/k_{app}(PabA + PabB) = allosteric activation factor) of analyzed mutant enzymes. (B) Mapping of residues with an allosteric activation factor <1.5 on the homology model of *E. coli* ADCS (PabA is depicted in cyan, and PabB is depicted in blue). Allosterically important positions are shown as spheres (C_α), and pathways are indicated as edges connecting them. Magnesium (Mg^{2+}) in the active site of PabB is shown as sphere as well. The catalytic triad *a*C79–*a*H168–*a*E170 and the substrates glutamine and chorismate (CH) are shown as sticks. All-atom RMSD between our *E. coli* ADCS model and the crystal structure of *S. solfataricus* AS, which was used for modeling, is 1.7 Å.

Using this classification, we found a putative network of conserved, mostly hydrogen-bonded residues that reach from the chorismate binding site in PabB to the active site of PabA. Interestingly, this allosteric communication network appears to be split into four branches: Starting from the chorismate binding site in PabB, these branches lead to (i) the oxyanion hole motif *a*P51–*a*G52–*a*P53, to (ii) the catalytic triad *a*C79–*a*H168–*a*E170, and to (iii + iv) residues involved in glutamine binding at the PabA glutaminase active site.
The branch that leads to the oxyanion hole stretch *a*P51–*a*G52–*a*P53 supposedly senses the presence of chorismate via its hydrophobic interaction with *b*I367 located near the C4-atom of chorismate. Through a van der Waals interaction with *b*Y112, the signal might then be propagated via backbone interactions of the helix formed by residues *b*D113– *b*L114–*b*G115–*b*R116 -*b*R117–*b*F118 and ultimately to *b*E119. Residue *b*E119 is located at the PabB–PabA interface and is hydrogen bonded to *a*R30. Via *a*R30, the signal is further transferred to the sequence stretch *a*Y8–*a*D9–*a*S10 adjacent to the oxyanion hole motif (Figure 2.3 B, purple).
The branch that leads to the catalytic triad *a*C79–*a*H168–*a*E170 presumptively senses the presence of chorismate via *b*E302, which is part of the conserved magnesium-binding site that coordinates the carboxylate group of chorismate. Via *b*E302 and the inter-domain hydrogen bonding network (Figure 2.8), the signal is ultimately transferred to *a*S171, which is located adjacent to the catalytic residues *a*H168 and *a*E170 (Figure 2.3 B, bright green).
One branch that leads to glutamine binding residues apparently senses the presence of chorismate via *b*K298, which interacts with residues of the conserved magnesium-binding site (i.e., *b*E439 and *b*E436). The signal is then propagated via *b*A301 and *a*H101 to the glutamine binding residues *a*R126, *a*H128, *a*S129, and *a*Q166 as well as to *a*L130, which is involved in ammonia tunnel formation (Figure 2.3 B, dark green).
The second branch that leads to glutamine binding residues reputedly senses the presence of chorismate via *b*I367 (described above) and *b*G369 and transfers the allosteric signal via *b*R374 and *b*D208 and ultimately to *b*G207, which is involved in glutamine binding at the glutaminase active site (Figure 2.3 B, pink).

2.3.4 Analysis of a PabA Mutant with Increased Basal Glutaminase Activity

Strikingly, PabA mutant *a*T125A shows a 10-fold acceleration of basal glutaminase activity [k_{app}(PabA) = 0.04 s^{-1}] compared to the wild-type enzyme [k_{app}(PabA) = 0.004 s^{-1}] (Table 2.5). As the allosteric activation factor (Figure 2.3 A) and catalytic parameters for the glutamine-dependent chorismate turnover are almost identical to wild-type ADCS (Tables 2.5 and 2.9), the wild-type *a*T125 residue seems not to be involved in the allosteric network, glutamine binding, or ammonia tunnel formation. Residue *a*T125 is hydrogen-bonded to *a*S171, an allosteric residue located adjacent to the catalytic residues *a*H168 and *a*E170 (Figure 2.4 A). The drastically enhanced basal glutaminase activity upon removal of this hydrogen bond in the *a*T125A mutant enzyme suggests that the relative positioning of *a*S171 with respect to the catalytic triad is

crucial for glutaminase activity. We thus further analyzed the interactions of *a*S171 to other residues in ADCS. As part of the inter-domain hydrogen bonding network, *a*S171 is also hydrogen bonded to the interaction hotspot *b*D308 (Figure 2.8). We generated mutant enzyme *b*D308E and monitored its ability to form stable ADCS complexes and to allosterically stimulate PabA activity. Strikingly, *b*D308E was not able to form stable ADCS complexes but led to a slightly enhanced k_{app}(PabA + PabB) and an allosteric activation factor of 1.2 (Tables 2.4 and 2.5). This finding indicates that this mutant might form a transient or weak interaction that affects the positioning of *a*S171 relative to the catalytic triad. We conclude that the corresponding wild-type residue *b*D308 undergoes a structural change in the course of signal propagation and might thus be a key residue for both complex formation and allosteric glutaminase activation within ADCS (Figure 2.4 B).

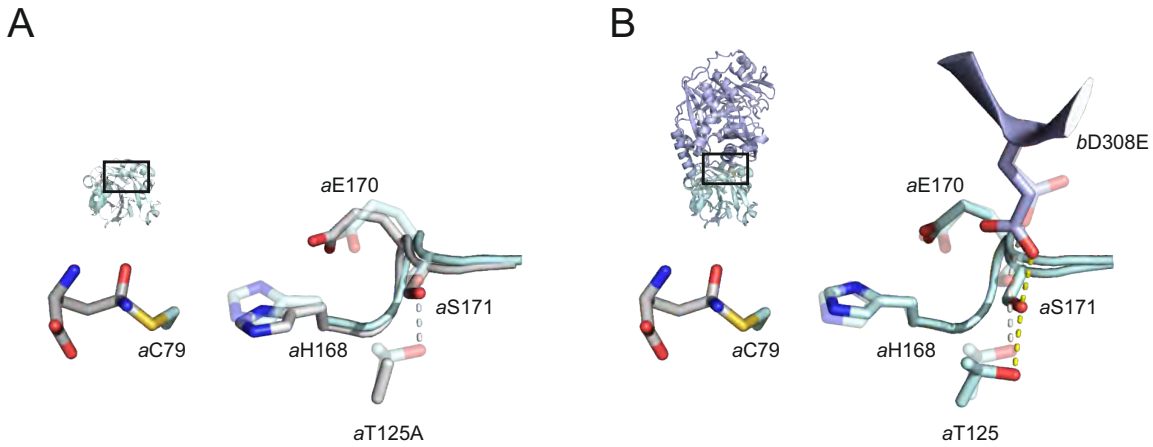

Figure 2.4: Activated variants of ADCS. (A) Putative structural changes in the *a*T125A mutant enzyme: *a*T125 is hydrogen bonded to *a*S171 in wild-type PabA (transparent). The loss of the hydrogen bond toward *a*S171 in the *a*T125A mutant might allow for the movement of the loop *a*H168–*a*P169–*a*E170–*a*S171 and thereby enhance basal glutaminase activity by reducing the *a*C79–*a*H168 distance (solid). (B) Putative structural changes in the *b*D308E mutant enzyme: *b*D308 is hydrogen-bonded to *a*S171 in wild-type ADCS (transparent). A potential movement of *b*D308 in the course of allosteric signaling is mimicked through the *b*D308E mutation and might result in bending of the loop *a*H168–*a*P169–*a*E170–*a*S171 to constitutively activate the glutaminase subunit (solid).

2.4 Discussion

Our study demonstrates that glutamine hydrolysis at the PabA subunit of ADCS is stimulated by the presence of chorismate at the PabB subunit via a conserved allosteric communication network. Starting from the chorismate binding site in PabB, the network splits into four branches that propagate the allosteric signal via mostly hydrogen-bonded residues to (i) the oxyanion hole motif *a*P51–*a*G52– *a*P53, (ii) the catalytic triad *a*C79–*a*H168–*a*E170, and (iii) glutamine binding residues at the PabA active site, respectively. In more general terms, chorismate might shift the enzyme complex from a less activated ensemble of conformational states to a more activated

ensemble (Motlagh et al., 2014). The deactivating effect observed in some mutants might thus result from the stabilization of the less activated ensemble by chorismate in these particular contexts.

In the following, we will discuss our findings in light of previously hypothesized activation mechanisms for different class I glutamine amidotransferase complexes. A hallmark feature of class I glutaminases is the catalytic triad composed of Cys–His–Glu, where Cys acts as nucleophile and His as general acid/base in the catalytic cycle (Figure 2.5).

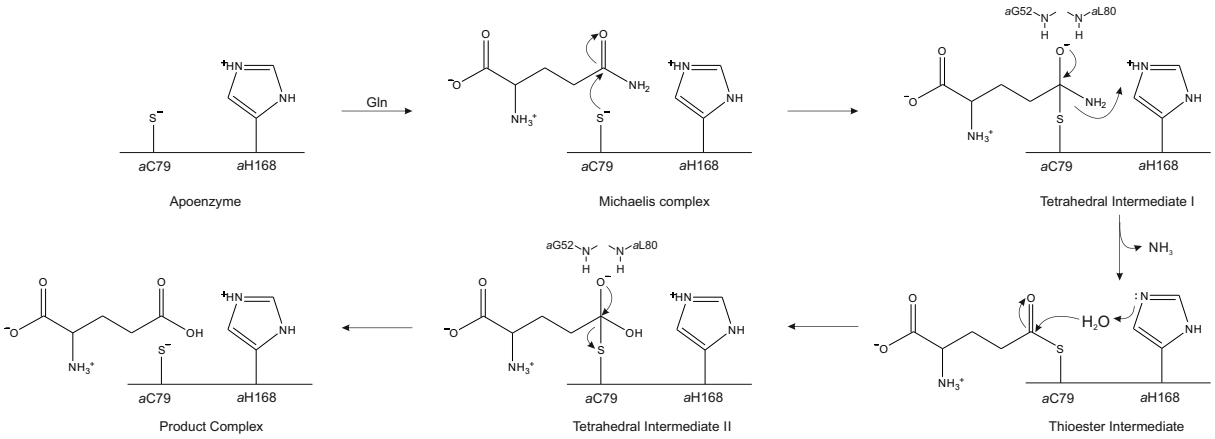

Figure 2.5: Reaction mechanism of class I glutaminases. Numbering of the essential Cys and His residues has been adapted to *ec*PabA. The Glu170 residue of the catalytic triad is not shown for simplicity. The mechanism was adopted from (Thoden et al., 1999).

Glutamine hydrolysis is thereby initiated by the attack of the thiolate anion of *a*C79 (nomenclature based on *E. coli* PabA) onto the carbonyl side-chain carboxamide of glutamine to form the tetrahedral intermediate I. This intermediate is stabilized by an oxyanion hole (in ADCS formed by backbone amides of *a*G52 and *a*L80) and collapses upon protonation of the amino group by the general acid *a*H168 into ammonia and the thioester intermediate. To complete the catalytic cycle, the thioester intermediate is hydrolyzed by an activated water molecule via the tetrahedral intermediate II.

Studies on ImGPS from *Thermotoga maritima* (Rivalta et al., 2012; Lipchock and Loria, 2010) and pyridoxal 5′-phosphate synthase (PS) from *B. subtilis* (Strohmeier et al., 2006) have indicated that allosteric signaling transforms the glutaminase active site from a catalysis *incompetent* to a catalysis *competent* conformation by inducing the formation of the oxyanion hole. Based on correlated motion NMR analysis and MD simulations of ImGPS, it was postulated that substrate binding to the synthase subunit HisF ultimately induces a 180° backbone flip of residue V51 in the glutaminase subunit HisH. As a result, the backbone amide of G50, which is part of the oxyanion hole, would become competent to stabilize the tetrahedral intermediates I/II. Likewise, the comparison of the crystal structures of the isolated and the associated subunits of PS has also indicated that complex formation results in a backbone flip of residue G46 in the glutaminase subunit, bringing the backbone amide of the neighbored G47 into a catalysis-competent conformation. Whereas the oxyanion hole motifs in both ImGPS (P49–G50–V51)

and PS (P45–G46–G47) theoretically allow for the proposed, energetically demanding backbone flip, in ADCS the oxyanion hole motif is composed of a highly conserved *a*P51–*a*G52–*a*P53 motif, where rotation of *a*G52 around the adjacent proline residue is not possible. This indicates that more subtle reorientations lead to a catalysis competent conformation in PabA. These findings for ADCS are in line with those for *Saccharomyces cerevisiae* ImGPS (Chaudhuri et al., 2003; Myers et al., 2005; Amaro et al., 2007), *E. coli* carbamoylphosphate synthetase (Thoden et al., 1999), and *E. coli* cytidine triphosphate synthetase (Goto et al., 2004) that provide no evidence for a backbone flip in their oxyanion hole motifs.

Moreover, in contrast to the postulated backbone flip in ImGPS from *T. maritima*, findings for the same enzyme from our laboratory suggested that the oxyanion hole of the glutaminase subunit HisH is in a catalysis-*competent* conformation even in the absence of substrate binding to the synthase HisF (List et al., 2012b). The same study showed that the mutation of HisH residues Y138 and K181 to alanines resulted in high constitutive glutaminase activity, suggesting that these amino acids are involved in the allosteric signaling pathway. Interestingly, Y138 and K181 correspond to the interaction hotspot *a*Y127 and the allosterically important residue *a*S171 identified in ADCS, respectively. Given the importance of the interaction between *a*Y127/*a*S171 and *b*D308 in ADCS, the effect of the mutations Y138A and K181A might be due to an impaired interaction with the conserved aspartate residue D98 of HisF, which corresponds to *b*D308 in ADCS. As this interaction is far apart from the oxyanion motif, it is tempting to speculate that these residues might influence the catalytic triad directly.

The analysis of two constitutively active TrpG glutaminase mutant enzymes (T129Y and T129F) of AS supports this notion, as the catalytic Cys-His distance is reduced in these mutants (List et al., 2012a). Interestingly, the position of T129 corresponds to *a*T125 in PabA, whose mutation to alanine also results in drastically increased basal glutamine hydrolysis. Taken together, the data obtained from the activated mutants of HisH, TrpG, and PabA indicate that a reorientation within the catalytic triad crucially contributes to glutaminase stimulation.

To conclude, our data on the allosteric communication pathway within ADCS allow us to bundle conclusions and hypotheses drawn from different laboratories on various class I GATases. Instead of attributing the allosteric activation mechanism of class I GATases exclusively to either the formation of the oxyanion hole or the reduction of distance between catalytic residues, we hypothesize an activation mechanism based on the combination of proper positioning of the oxyanion hole and glutamine-binding residues along with a distance reduction between the catalytic Cys-His residues (Figure 2.6).

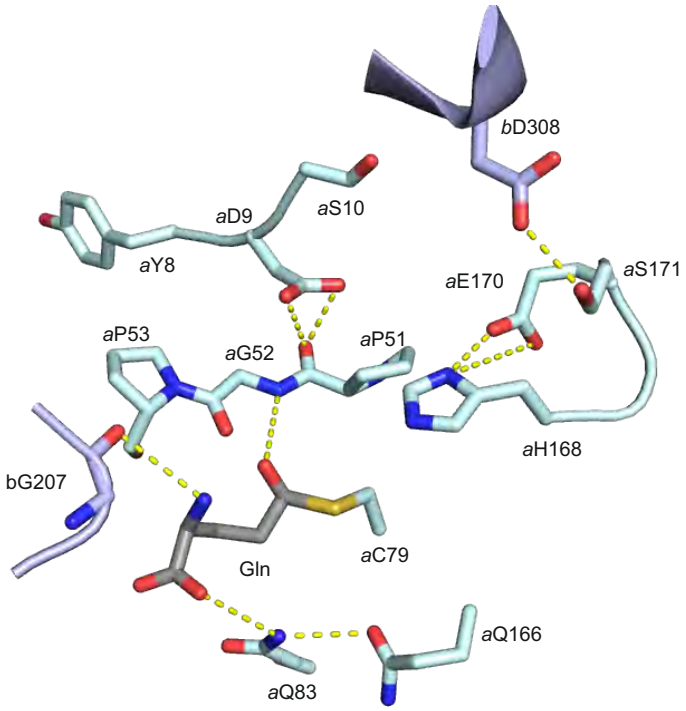

Figure 2.6: Endpoints of the allosteric communication pathways in ADCS. The oxyanion hole (*a*P51–*a*G52–*a*P53) is positioned by *a*Y8, *a*D9, and *a*S10, where the substrate-induced movement of the carboxylate side chain of *a*D9 might lead to proper orientation of the oxyanion hole through interaction with the carbonyl group of *a*G52. Movement of *b*D308 toward *a*S171 might lead to a reduction of the *a*C79–*a*H168 distance by changes in the relative orientation of the *a*H168–*a*P169–*a*E170 loop. The substrate glutamine (Gln, shown as thioester intermediate) interacts via its α-amino group with the main chain carbonyl group of *b*G207, whereas its α-carboxylate group forms a hydrogen bond with the side chain of *a*Q83, which is coordinated by *a*Q166.

2.5 Material and Methods

2.5.1 Cloning and Mutagenesis

The genes of *ec*PabA and *ec*PabB as cloned into the pET21a expression plasmid were available from a previous study (Plach et al., 2017). Single amino acid mutant enzymes (Table 2.11) were produced using a modified QuickChange mutagenesis protocol (Wang and Malcolm, 1999) with the primers listed in Table 2.8.

2.5.2 Gene Expression and Protein Purification

Proteins were produced by gene expression in *E. coli* BL21-Gold (DE3) cells as previously described (Plach et al., 2017). In brief, overnight cultures of individual clones were used to

inoculate 1 L (*ec*PabA variants) or 2 L (*ec*PabB variants) of Luria broth medium supplemented with 150 µg/mL ampicillin. Cells were grown at 37 °C to an OD_{600} of 0.6 and then cooled to 25 °C. Expression was induced by adding 0.5 mM IPTG and growth was continued overnight at 20 °C. Cells were harvested by centrifugation (2700 g, 4 °C), suspended in 50 mM Tris–HCl (pH 7.5), 300 mM potassium chloride, and 10 mM imidazole, and lyzed by sonification. The insoluble fraction was removed by centrifugation (23,000 g, 4 °C), and the soluble extracts were filtered through a 0.8-µm membrane. Supernatants containing the C-terminal hexahistidine-tagged proteins were loaded onto a HisTrapFF crude column (5 mL, GE Healthcare), which had been equilibrated with suspension buffer, and eluted from the column by applying a linear gradient of 10–750 mM imidazole. Enzyme-containing fractions, as judged by SDS-PAGE, were pooled and further purified by preparative gel filtration [Superdex 75 HiLoad 26/60, 320 mL, GE Healthcare, 50 mM Tris–HCl (pH 7.5), 50 mM KCl, 5 mM $MgCl_2$, 2 mM DTT, 4 °C]. Elution fractions were analyzed by SDS-PAGE, and the fractions containing pure protein were pooled. The enzymes were finally concentrated to 50–150 µM and flash frozen in liquid nitrogen. Protein concentrations were determined by measuring the absorbance at 280 nm using the molar extinction coefficient calculated via ExPASy ProtParam (http://web.expasy.org/ protparam/).

2.5.3 Ancestral Sequence Reconstruction of PabA

Methods of our standard protocol for sequence selection (Straub and Merkl, 2019) were applied to a precompiled set of 2825 concatenated PabA and PabB sequences (Plach et al., 2017). A subset promising a robust tree and consisting of 59 concatenated sequences from Firmicutes, Fusobacteria, Proteobacteria, and the archaeal phylum Halobacteriales were chosen for ASR. A multiple sequence alignment was generated by means of MAFFT (Katoh and Standley, 2013) and solely for the computation of a phylogenetic tree that guides the subsequent reconstruction, positions containing more than 50% gaps were removed by using GBlocks (Castresana, 2000). The phylogenetic tree was computed with the help of pb (version 3.3 of PhyloBayes (Lartillot et al., 2009)) and the options -cat -gtr and by launching four independent Monte Carlo Markov Chains of length 50,000 to ensure convergence. The quality of mixing was assessed by computing for each pair of chains the discrepancy index (maxdiff, which was <0.03 in all cases) by means of bpcomp and the minimum effective size (which was >200 in all cases) with tracecomp. As all results indicated the convergence of the chains, a consensus tree was determined by means of readpb and a burn-in of 2000 (Figure 2.7). The phylogeny-aware multiple sequence aligner PRANK (Löytynoja and Goldman, 2008) with the option -showanc was applied to the full multiple sequence alignment and the consensus tree to deduce the position of gaps in the reconstructed sequences. Their amino acid compositions were calculated with the program ancestral from PhyloBayes using midpoint rooting and the PRANK phylogeny. For the three bacterial predecessors *anc*1PabA–*anc*3PabA, which were deduced from the concatenations, the amino acid sequences are listed in Table 2.10.

2.5.4 Crystallization, Data Collection, and Structure Determination

Crystals of *anc*2PabA were obtained at 16 °C by the hanging-drop vapor diffusion method with a 500-µL reservoir consisting of 20 % PEG 1500 and 40 % glycerol. One microliter of a 850-µM protein solution was mixed with 1 µL of reservoir solution, and crystals grew within 10 days. Data collection was done at Swiss Light Source, Switzerland, at beamline PXIII and PXI at cryogenic temperature. The data processing was done using XDS (Adams et al., 2002; Kabsch, 1993), and the data quality assessment was done using phenix.xtriage. Molecular replacement was performed with Phaser (Mccoy et al., 2007) within the CCP4i (Potterton et al., 2004) suite using a homologymodel of *anc*2PabA (generated with I-TASSER (Zhang and Skolnick, 2005; Roy et al., 2010; Yang et al., 2015) as template. Initial refinement was performed using REFMAC (Murshudov et al., 1997). The model was further improved in several refinement rounds using automated restrained refinement with the program PHENIX (Adams et al., 2002) and interactive modeling with Coot (Emsley and Cowtan, 2004). The refinement statistics are listed in Table 2.6. The final model was analyzed using the program MolProbity (Davis et al., 2007).

2.5.5 Analysis of Complex Formation Between Different Synthases and Glutaminases

The ability of PabA and PabB variants to form heteromeric complexes was examined by size exclusion chromatography as previously described (Plach et al., 2017). In brief, the experimental setup of SEC comprised Superdex 75 10/300 GL column (GE Healthcare) operated on an ÄKTAmicro system (GE Healthcare) connected to an ALIAS autosampler (Spark Holland). The system was operated at 25 °C with a flow rate of 0.5 mL/min of degassed buffer [50 mM Tris–HCl (pH 7.5), 150 mM KCl, 5 mM $MgCl_2$] and was calibrated with conalbumin, ovalbumin, carbonic anhydrase, ribonuclease A, and aprotinin from the GE Healthcare SEC Low-Molecular-Weight as well as the SEC High-Molecular-Weight calibration kit. Individual synthases and glutaminases were assayed at a concentration of 50 µM (applied volume 50 µL). For analysis of complex formation, synthases and glutaminases were equimolarly mixed to a final concentration of 50 µM.

2.5.6 Steady-State Enzyme Kinetics

The glutaminase activity was measured spectrophotometrically in a coupled enzymatic assay as previously described (Plach et al., 2017). In brief, glutamate formed by the glutaminase was converted to α-ketoglutarate by glutamate-dehydrogenase with simultaneous reduction of NAD^+ to NADH. A standard assay contained 50 mM Tricine–KOH buffer (pH 8.0), 5 mM $MgCl_2$, 1 mM DTT, 10 mM NAD^+, 1 mg/mL glutamate-dehydrogenase, and 20 mM glutamine. Following preincubation, 1 µM glutaminase PabA was added, and the reaction was monitored at 340 nm

and 25 °C for 20 min. After making sure that the progress curve proceeded with a constant slope, 3 µM synthase PabB or 3 µM synthase PabB + 200 µM chorismate were added and the reaction was again monitored for at least 10 min. The slopes of the linear parts of the progress curves before and after the addition of the synthase/synthase + chorismate were used to calculate the apparent turnover rate upon the addition of the synthase/synthase + chorismate. The ratio of the apparent turnover rates in the presence and absence of chorismate was used to calculate allosteric activation factors. Slopes were determined and calculations performed within a custom Python script.
The PabB reaction was measured at 25 °C using an assay monitoring para-aminobenzoic acid fluorescence (excitation 320 nm, emission 350 nm) (Plach et al., 2017). For this purpose, the PabB product 4-amino-4-deoxychorismate was converted *in situ* to para-aminobenzoic acid by a molar excess of 4-amino-4-deoxychorismate lyase (PabC). A standard glutamine-depending assay contained 100 mM potassium phosphate buffer (pH 7.0), 5 mM $MgCl_2$, 1 mM DTT, 10 µM PabC, 200 µM CH, and 1.5 µM PabB and 0.5 µM PabA. After preincubation, 0–10 mM glutamine was added. For each individual substrate concentration, progress curves were collected and fitted to the Michaelis–Menten equation in a custom Python script to derive k_{cat} and ${K_M}^{Gln}$.

2.5.7 Thermal Stability of Purified Proteins

Melting temperatures of purified proteins were determined with nano-differential scanning fluorimetry in a Prometheus NT.48 (NanoTemper, Munich) at the facilities of 2bind molecular interactions in Regensburg. Typically, 10 µL of a 100-µM protein solution was loaded into glass capillaries, and intrinsic tryptophan fluorescence emission intensities F330 nm and F350 nm were measured from 20 to 95 °C. The maxima of first derivatives of F330 nm/F350 nm were used to derive the melting temperature T_M at which half of the protein is denatured.

2.5.8 Accession Numbers

*ec*PabA_WT—NCBI Reference Sequence: WP_115194528.
*ec*PabB_WT—NCBI Reference Sequence: WP_000854958.
*anc*2PabA—PDB ID: 6QUR

2.5.9 CRediT Authorship Contribution Statement

Florian Semmelmann: Conceptualization, Writing - original draft. Kristina Straub: Investigation, Writing - original draft. Julian Nazet: Investigation. Chitra Rajendran: Investigation, Writing - original draft. Rainer Merkl: Conceptualization, Supervision, Writing - review & editing. Reinhard Sterner: Conceptualization, Supervision, Writing - review & editing.

2.5.10 Acknowledgments

F.S. was supported by a doctoral fellowship from the Konrad-Adenauer-Stiftung. We thank Christiane Endres, Sonja Fuchs, Sabine Laberer, Ulrike Stöckl, and Jeannette Ueckert for expert technical assistance. We thank 2bind molecular interactions GmbH for access to Prometheus NT.48 and consumables.

Author Contributions

Conceptualization: F.S., R.M., R.S. - Investigation: F.S., K.S., J.N., C.R. - Supervision: R.M., R.S. - Writing: - original draft: F. S., K.S., C.R. - Writing - review & editing: R.M., R.S.

Declaration of Competing Interest

The authors declare that they have no competing financial interests.

2.5.11 Appendix A. Supplementary data

Supplementary data to this article can be found online at https://doi.org/10.1016/j.jmb.2019.05.021.

2.5.12 Keywords

allostery; ancestral sequence reconstruction; bi-enzyme complex; catalytic triad; glutamine amidotransferases

2.5.13 Abbreviations Used

GATases, glutamine amidotransferases; ADCS, aminodeoxychorismate synthase; AS, anthranilate synthase; ImGPS, imidazole glycerol phosphate synthase.

2.6 Supplemental Information

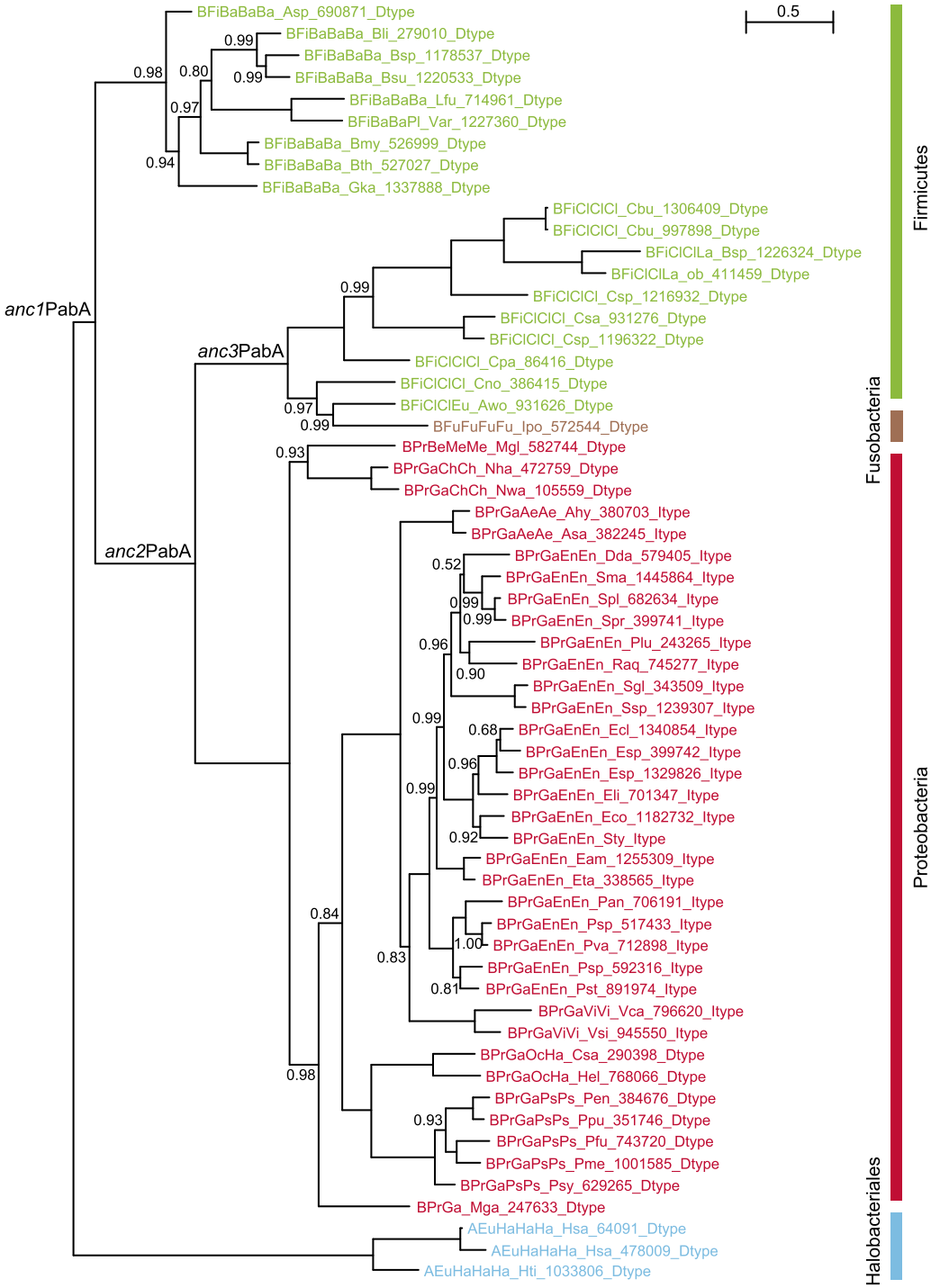

Figure 2.7: Phylogenetic tree used for sequence reconstruction of ancestral PabA proteins. The tree was determined for 59 concatenated PabA and PabB sequences from Firmicutes, Fusobacteria, Proteobacteria, and Halobacteriales. For all internal nodes, the posterior probability was determined; their values are only given, if below 1.0. The length of the horizontal bar corresponds to 0.5 substitutions per site.

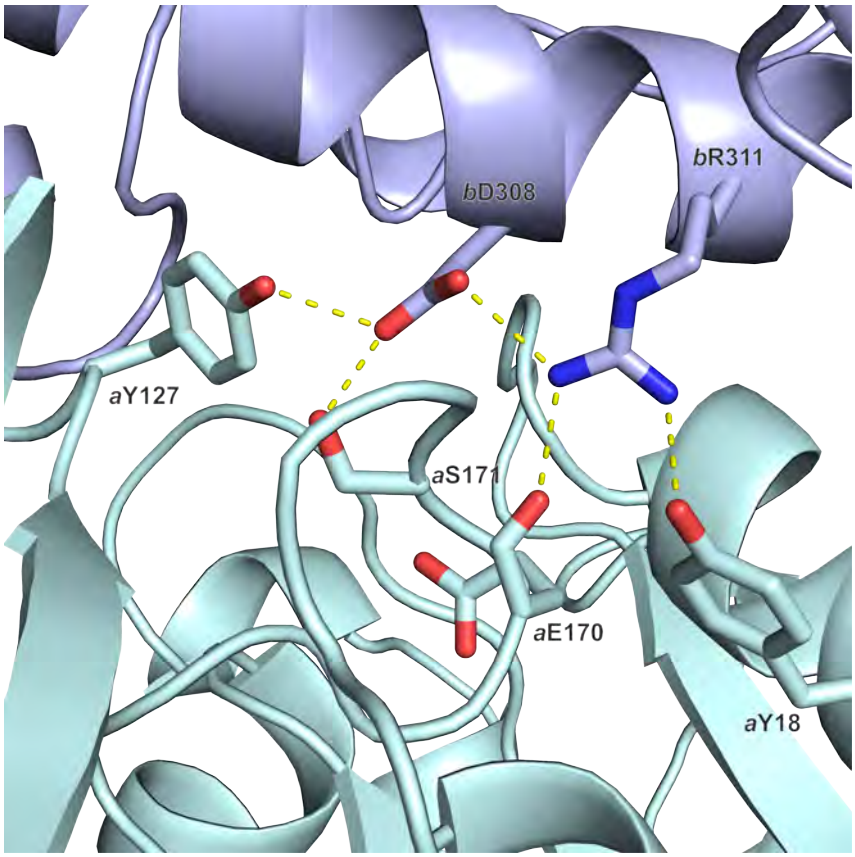

Figure 2.8: Inter-domain hydrogen bonding network of ADCS. Side chains involved in interactions between PabA and PabB are shown as sticks and the carbonyl backbone is shown for *a*E170.

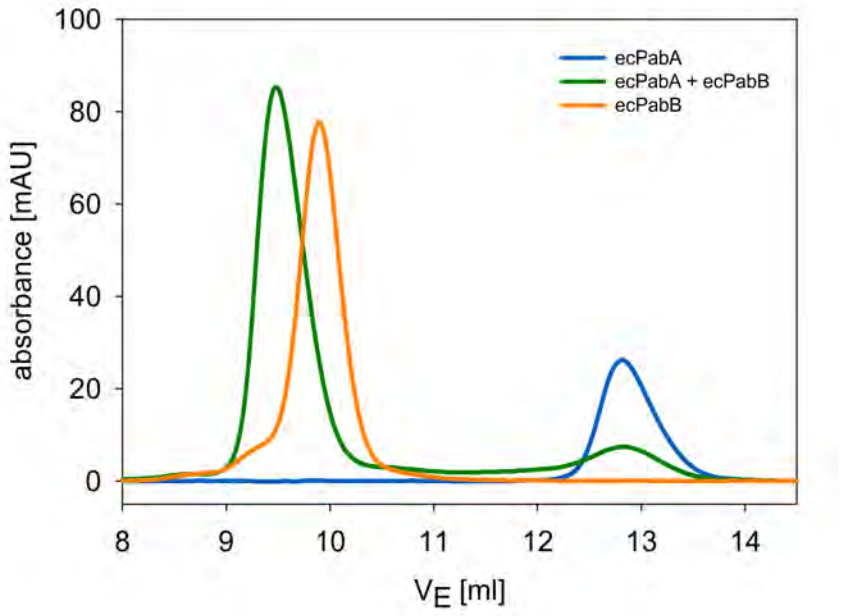

Figure 2.9: Standard size exclusion chromatography trace for *E. coli* ADCS. Analytical size exclusion chromatography with wild-type *ec*PabA, *ec*PabB and an equimolar mixture of both. The proteins (50 µM, subunit concentration) were applied to a S75 analytical column equilibrated with 50 mM TRIS pH 7.5, 150 mM KCl, 5 mM $MgCl_2$. Elution was performed at a flow rate of 0.5 mL/min and followed by measuring the absorption at 280 nm, which was plotted against the elution volume (V_E). *ec*PabA is depicted in blue, *ec*PabB in orange, and the mixture of *ec*PabA and *ec*PabB in green.

Table 2.1: Thermal stability of *anc*1-3PabA and modern PabA enzymes. Modern PabA enzymes from *Serratia marcescens (sm)*, *Bacillus subtilis (bs)*, *E. coli (ec)*, and *Pseudomonas putida (pp)* were available from a previous study (Plach et al., 2017).

Enzyme	T_m value (°C)
*anc*1PabA	80.1 ± 0.05
*anc*2PabA	58.6 ± 0.20
*anc*3PabA	65.5 ± 0.05
*sm*PabA	52.3 ± 0.08
*bs*PabA	42.1 ± 0.02
*pp*PabA	50.3 ± 0.02
*ec*PabA	51.6 ± 0.08

Table 2.2: Multiple sequence alignment of ancestral and modern PabA enzymes. Sequences were aligned with MAFFT (Katoh and Standley, 2013). Conserved amino acids are indicated by asterisks, similar amino-acids are indicated as colon (PAM 250 score > 0.5) or dots (PAM 250 score ≤ 0.5) at the bottom of each column.

```
anc1PabA        MILMIDNYDSFTYNLVQYLGELGEEVVVKRNDEITIAEIEQLKPDFLVISPGPCTPNEAG
anc2PabA        MILMIDNYDSFTYNLVQYLGELGEEVVVYRNDEITIAEIEKLKPDHLVISPGPCTPNEAG
anc3PabA        MLLMIDNYDSFTYNLVQYLGELGEDVCVYRNDEITIAEIEALRPDHLVISPGPCTPNEAG
bsPabA          MILMIDNYDSFTYNLVQYLGELGEELVVKRNDSITIDEIEELSPDFLMISPGPCSPDEAG
ppPabA          MLLMIDNYDSFTYNVVQYLGELGAEVKVIRNDELTIAQIEALNPERIVVSPGPCTPSEAG
smPabA          MLLLIDNYDSFTYNLYQYFCELGAEVMVKRNDELQLADIERLAPQHLVISPGPCTPNEAG
ecPabA          MILLIDNYDSFTWNLYQYFCELGADVLVKRNDALTLADIDALKPQKIVISPGPCTPDEAG
                *:*:********:*: **: *** :: * *** : : :*: * *: :::*****:*.***

anc1PabA        ISLEVIKHFAGKIPIFGVCLGHQSIAQVFGGEVVRAERLMHGKTSPIFHDGKGIFAGLPN
anc2PabA        ISLEVIKHFAGKIPILGVCLGHQSIGQAFGGKIVRAKQVMHGKTSEIYHNNKGVFKGLNN
anc3PabA        ISLAVIRHFAGKIPILGVCLGHQSIGQAFGGRIVRAKQVMHGKTSQVYHNNKGVFAGLNN
bsPabA          ISLEAIKHFAGKIPIFGVCLGHQSIAQVFGGDVVRAERLMHGKTSDIEHDGKTIFEGLKN
ppPabA          VSIEAILHFAGKLPILGVCLGHQSIGQAFGGDVVRARQVMHGKTSPVYHRDLGVFASLNN
smPabA          ISLAAIRHFAGKLPILGVCLGHQALGQAFGAEVVRARAVMHGKTSAIRHLGVGVFRGLND
ecPabA          ISLDVIRHYAGRLPILGVCLGHQAMAQAFGGKVVRAAKVMHGKTSPITHNGEGVFRGLAN
                :*: .* *:**::**:*******::.*.**. :***  :****** : * .  :* .* :

anc1PabA        PFTATRYHSLIVKRETLPDCLEVTAWTE--EG---EIMGIRHKTLPIEGVQFHPESILTE
anc2PabA        PFEATRYHSLVVERETLPDCLEITAWTETDEG---EIMGIRHKTLPIEGVQFHPESILTE
anc3PabA        PFEATRYHSLVIERETLPDCLEITAWTETDTGELDEIMGIRHKTLPIEGVQFHPESILTE
bsPabA          PLVATRYHSLIVKPETLPSCFTVTAQTK--EG---EIMAIRHNDLPIEGVQFHPESIMTS
ppPabA          PLTVTRYHSLVVKRETLPDCLEVTAWTSHADGSVDEIMGLRHKTLNIEGVQFHPESILTE
smPabA          PLTVTRYHSLVLKADTLPDCFEVTAWSER-DGVRDEIMGIRHRTLALEGVQFHPESVLSE
ecPabA          PLTVTRYHSLVVEPDSLPACFDVTAWSE-----TREIMGIRHRQWDLEGVQFHPESILSE
                *: .******::: ::** *: :** :.       ***.:**.   :*********:::.

anc1PabA        HGHELLKNFITLYRKK----
anc2PabA        QGHELLKNFLKE-------
anc3PabA        QGHDLLRNFLKQ-------
bsPabA          FGKEMLRNFIETYRKEVIA
ppPabA          QGHELFANFLKQTGGRR--
smPabA          QGHQLLDNFLNR-------
ecPabA          QGHQLLANFLHR-------
                 *:::: **:
```

Table 2.3: Sequence identities/similarities between analyzed PabA enzymes. The %-sequence identities are shown and the %-sequence similarities are shown in brackets.

	***anc1*PabA**	***anc2*PabA**	***anc3*PabA**	***sm*PabA**	***bs*PabA**	***pp*PabA**	***ec*PabA**
***anc1*PabA**	100%	-	-	-	-	-	-
***anc2*PabA**	86% (93%)	100%	-	-	-	-	-
***anc3*PabA**	79% (88%)	90% (95%)	100%	-	-	-	-
***sm*PabA**	68% (81%)	70% (83%)	71% (82%)	100%	-	-	-
***bs*PabA**	82%(87%)	73% (84%)	67% (79%)	61% (77%)	100%	-	-
***pp*PabA**	73% (83%)	76% (86%)	77% (87%)	71% (83%)	63% (75%)	100%	-
***ec*PabA**	68% (85%)	69% (85%)	66% (81%)	76% (85%)	61% (81%)	65% (81%)	100%

Table 2.4: SEC experiments to determine complex formation. The apparent molecular weight (MW_{app}) was determined based on a calibration curve of standard proteins (ovalbumine, carbonic anhydrase, ribonuclease A, conalbumin, ovalbumin and aldolase). The calculated molecular weight (MW_{calc}) derives from the amino-acid sequence and was determined via Expasy Protparam.

Synthase	**Glutaminase**	**MW_{app} [kDa]**	**MW_{calc} [kDa]**	**Deduced oligomeric state**
***E. coli* ADCS**				
bY112A	aWT	63.5	73.9	B:A dimer
bE119A	aWT	62.3	73.9	B:A dimer
bG207A	aWT	61.9	73.9	B:A dimer
bD208A	aWT	63.3	73.9	B:A dimer
bV212A	aWT	64.1	73.9	B:A dimer
bN213A	aWT	63.7	73.9	B:A dimer
bG275A	aWT	63.2	73.9	B:A dimer
bT276A	aWT	64.1	73.9	B:A dimer
bK298A	aWT	62.6	73.9	B:A dimer
bR300A	aWT	66.1	73.9	B:A dimer
bA301V	aWT	63.2	73.9	B:A dimer
bE302A	aWT	64.5	73.9	B:A dimer
bM305A	aWT	62.1	73.9	B:A dimer
bD308A	aWT	-	-	no complex
		54.2	52.0	bD308A monomer
		18.8	21.9	PabA monomer
bD308E	aWT	-	-	no complex
		54.4	52.0	bD308E monomer
		18.8	21.9	PabA monomer
bL309A	aWT	58.3	73.9	B:A dimer
bR311A	aWT	-	-	no complex
		53.8	52.0	bR311A monomer
		18.8	21,9	PabA monomer
bN312A	aWT	63.8	73.9	B:A dimer
bI367A	aWT	65.8	73.9	B:A dimer
bG369A	aWT	66.2	73.9	B:A dimer
bA370V	aWT	64.4	73.9	B:A dimer
bK372A	aWT	67.3	73.9	B:A dimer
bR374A	aWT	63.3	73.9	B:A dimer
bA423V	aWT	66.5	73.9	B:A dimer
bG424A	aWT	63.3	73.9	B:A dimer

bG426A	aWT	62.7	73.9	B:A dimer
bV428A	aWT	61.2	73.9	B:A dimer
bWT	aD6A	58.3	73.9	B:A dimer
bWT	aY8A	61.1	73.9	B:A dimer
bWT	aD9A	61.2	73.9	B:A dimer
bWT	aS10A	63.6	73.9	B:A dimer
bWT	aF11A	59.0	73.9	B:A dimer
bWT	aR30A	60.9	73.9	B:A dimer
bWT	aP51A	64.1	73.9	B:A dimer
bWT	aP53A	63.1	73.9	B:A dimer
bWT	aT55A	62.8	73.9	B:A dimer
bWT	aM100A	59.6	73.9	B:A dimer
bWT	aH101A	62.2	73.9	B:A dimer
bWT	aG102A	62.1	73.9	B:A dimer
bWT	aK103A	60.9	73.9	B:A dimer
bWT	aT104A	60.6	73.9	B:A dimer
bWT	aT125A	62.7	73.9	B:A dimer
bWT	aR126A	62.1	73.9	B:A dimer
bWT	aY127A	-	-	no complex
		55.4	52.0	PabB monomer
		15.6	21,9	aY127A monomer
bWT	aH128A	65.2	73.9	B:A dimer
bWT	aS129A	63.3	73.9	B:A dimer
bWT	aL130A	62.5	73.9	B:A dimer
bWT	aQ166A	58.6	73.9	B:A dimer
bWT	aS171A	58.6	73.9	B:A dimer
bWT	aI172A	62.3	73.9	B:A dimer
bWT	PabA_WT	63.3	73.9	B:A dimer
Reconstructed, ancestral PabA				
bWT	*anc*1PabA	62.1	73.4	B:A dimer
bWT	*anc*2PabA	61.5	73.2	B:A dimer
bWT	*anc*3PabA	60.4	73.5	B:A dimer

Table 2.5: Stimulation of the PabA glutaminase activity by PabB or PabB + chorismate.

Glutaminase	Synthase	k_{app}(PabA) [s^{-1}]	k_{app}(PabA+PabB) [s^{-1}]	k_{app}(PabA+PabB+CH) [s^{-1}]	allosteric activation factor
***E. coli* ADCS**					
aD6A	bWT	n.d.	0.22 ± 0.01	0.070 ± 0.003	0.32 ± 0.03
aY8A	bWT	8.0 ± 0.8 x 10^{-3}	0.34 ± 0.02	0.34 ± 0.02	1.00 ± 0.12
aD9A	bWT	n.d.	0.270 ± 0.004	0.15 ± 0.01	0.56 ± 0.04
aS10A	bWT	5.0 ± 1.3 x 10^{-3}	0.54 ± 0.03	0.270 ± 0.003	0.50 ± 0.03
aF11A	bWT	3.0 ± 0.1 x 10^{-3}	0.20 ± 0.01	0.380 ± 0.002	1.90 ± 0.10
aR30A	bWT	3.0 ± 0.9 x 10^{-3}	0.51 ± 0.04	0.54 ± 0.04	1.14 ± 0.17
aP51A	bWT	1.0 ± 0.2 x 10^{-3}	0.13 ± 0.01	0.36 ± 0.01	2.77 ± 0.29
aP53A	bWT	3.0 ± 2.3 x 10^{-3}	0.13 ± 0.02	0.39 ± 0.02	3.00 ± 0.62
aT55A	bWT	2.0 ± 0.4 x 10^{-3}	0.35 ± 0.01	0.76 ± 0.20	2.17 ± 0.63
aM100A	bWT	3.0 ± 0.3 x 10^{-3}	0.11 ± 0.01	0.43 ± 0.02	3.91 ± 0.03
aH101A	bWT	3.0 ± 0.8 x 10^{-3}	0.40 ± 0.02	0.48 ± 0.02	1.20 ± 0.16
aG102A	bWT	n.d.	0.270 ± 0.003	0.65 ± 0.02	2.41 ± 0.02
aK103A	bWT	n.d.	0.191 ± 0.005	0.40 ± 0.05	2.10 ± 0.07
aT104A	bWT	n.d.	0.24 ± 0.01	0.54 ± 0.03	2.25 ± 0.22
aT125A	bWT	3.8 ± 0.9 x 10^{-2}	0.30 ± 0.02	0.63 ± 0.02	2.10 ± 0.21
aR126A	bWT	n.d.	0.28 ± 0.02	0.16 ± 0.01	0.57 ± 0.08
aY127A	bWT	n.d.	n.d.	n.d.	n.d.
aH128A	bWT	n.d.	0.49 ± 0.02	0.39 ± 0.02	0.80 ± 0.07
aS129A	bWT	2.0 ± 0.9 x 10^{-3}	0.51 ± 0.03	0.58 ± 0.01	1.14 ± 0.09
aL130A	bWT	n.d.	0.51 ± 0.04	0.271 ± 0.002	0.53 ± 0.04
aQ166A	bWT	n.d.	0.38 ± 0.02	0.23 ± 0.01	0.61 ± 0.06
aS171A	bWT	n.d.	0.159 ± 0.004	0.110 ± 0.004	0.69 ± 0.06

aI172A	bWT	$3.0 \pm 1.5 \times 10^{-3}$	0.34 ± 0.02	0.53 ± 0.02	1.56 ± 0.15
aWT	bY112A	$3.0 \pm 2.0 \times 10^{-3}$	0.47 ± 0.08	0.071 ± 0.001	0.15 ± 0.03
aWT	bE119A	$4.0 \pm 1.0 \times 10^{-3}$	0.56 ± 0.05	0.50 ± 0.04	0.89 ± 0.15
aWT	bG207A	$4.0 \pm 0.2 \times 10^{-3}$	0.45 ± 0.03	0.30 ± 0.01	0.67 ± 0.07
aWT	bD208A	$3.0 \pm 0.8 \times 10^{-3}$	0.54 ± 0.02	0.60 ± 0.01	1.11 ± 0.06
aWT	bV212A	$5.0 \pm 0.8 \times 10^{-3}$	0.04 ± 0.01	0.18 ± 0.003	4.10 ± 1.03
aWT	bN213A	$3.0 \pm 1.0 \times 10^{-3}$	0.100 ± 0.002	0.32 ± 0.02	3.20 ± 0.20
aWT	bG275A	$4.0 \pm 0.3 \times 10^{-3}$	0.33 ± 0.02	0.31 ± 0.01	0.94 ± 0.09
aWT	bT276A	$4.0 \pm 0.3 \times 10^{-3}$	0.112 ± 0.004	0.20 ± 0.01	1.82 ± 0.09
aWT	bK298A	$3.0 \pm 0.6 \times 10^{-3}$	0.30 ± 0.01	0.32 ± 0.01	1.07 ± 0.20
aWT	bR300A	$3.0 \pm 0.7 \times 10^{-3}$	0.33 ± 0.01	0.51 ± 0.03	1.55 ± 0.14
aWT	bA301V	$4.0 \pm 0.6 \times 10^{-3}$	0.42 ± 0.03	0.49 ± 0.05	1.17 ± 0.20
aWT	bE302A	$3.0 \pm 0.3 \times 10^{-3}$	0.168 ± 0.002	0.128 ± 0.005	0.76 ± 0.01
aWT	bM305A	$3.0 \pm 0.5 \times 10^{-3}$	0.37 ± 0.02	0.43 ± 0.03	1.16 ± 0.14
aWT	bD308A	$3.5 \pm 0.4 \times 10^{-3}$	0.03 ± 0.01	0.08 ± 0.01	2.66 ± 1.22
aWT	bD308E	$4.6 \pm 0.0 \times 10^{-3}$	0.29 ± 0.04	0.34 ± 0.06	1.17 ± 0.61
aWT	bL309A	$3.0 \pm 0.5 \times 10^{-3}$	0.20 ± 0.01	0.39 ± 0.01	1.95 ± 0.15
aWT	bR311A	$4.0 \pm 0.9 \times 10^{-3}$	0.13 ± 0.10	0.46 ± 0.01	3.54 ± 2.80
aWT	bN312A	$4.0 \pm 2.0 \times 10^{-3}$	0.25 ± 0.01	0.470 ± 0.005	1.88 ± 0.08
aWT	bI367A	$2.0 \pm 0.6 \times 10^{-3}$	0.42 ± 0.02	0.44 ± 0.03	1.05 ± 0.12
aWT	bG369A	$2.0 \pm 0.2 \times 10^{-3}$	0.19 ± 0.01	0.28 ± 0.01	1.52 ± 0.09
aWT	bA370V	$5.0 \pm 1.4 \times 10^{-3}$	0.207 ± 0.005	0.40 ± 0.02	1.90 ± 0.10
aWT	bK372A	$3.0 \pm 1.0 \times 10^{-3}$	0.13 ± 0.01	0.23 ± 0.01	1.77 ± 0.21
aWT	bR374A	$5.0 \pm 0.6 \times 10^{-3}$	0.21 ± 0.01	0.27 ± 0.01	1.29 ± 0.11
aWT	bA423V	$3.0 \pm 1.0 \times 10^{-3}$	0.152 ± 0.004	0.39 ± 0.03	2.60 ± 0.20
aWT	bG424A	$4.0 \pm 0.4 \times 10^{-3}$	0.165 ± 0.001	0.29 ± 0.02	1.81 ± 0.12

aWT	bG426A	$2.0 \pm 1.0 \times 10^{-3}$	0.160 ± 0.001	0.48 ± 0.04	3.00 ± 0.25
aWT	bV428A	$5.0 \pm 0.7 \times 10^{-3}$	0.100 ± 0.002	0.20 ± 0.04	2.00 ± 0.40
aWT	bWT	$4.0 \pm 0.6 \times 10^{-3}$	0.21 ± 0.01	0.58 ± 0.03	2.74 ± 0.27
Reconstructed, ancestral PabA					
*anc*1PabA	bWT	$1.2 \pm 0.2 \times 10^{-3}$	0.05 ± 0.01	0.13 ± 0.04	2.60 ± 1.32
*anc*2PabA	bWT	$7.0 \pm 0.2 \times 10^{-3}$	0.11 ± 0.01	0.26 ± 0.02	2.36 ± 0.40
*anc*3PabA	bWT	$1.3 \pm 0.2 \times 10^{-1}$	0.28 ± 0.01	0.40 ± 0.01	1.43 ± 0.09

n.d. = not detectable

Table 2.6: Data collection and refinement statistics for *anc*2PabA.

Wavelength (Å)	1
Resolution range	39.73 - 1.792 (1.856 - 1.792)
Space group	P 21 21 21
Unit cell	47.755 58.39 71.583 90 90 90
Total reflections	251114 (22159)
Unique reflections	19372 (1880)
Multiplicity	13.0 (11.8)
Completeness (%)	99.87 (99.16)
Mean I/sigma(I)	23.52 (1.27)
Wilson B-factor	33.96
R-merge	0.06472 (1.935)
R-meas	0.06743 (2.023)
R-pim	0.01866 (0.5803)
CC1/2	1 (0.6)
CC*	1 (0.866)
Reflections used in refinement	19365 (1880)
Reflections used for R-free	969 (94)
R-work	0.2145 (0.3364)
R-free	0.2672 (0.3440)
CC(work)	0.961 (0.763)
CC(free)	0.917 (0.660)
Number of non-hydrogen atoms	1632
macromolecules	1519
solvent	113
Protein residues	193
RMS(bonds)	0.007
RMS(angles)	0.89
Ramachandran favored (%)	97.38
Ramachandran allowed (%)	2.62
Ramachandran outliers (%)	0.00
Rotamer outliers (%)	0.00
Clashscore	3.96
Average B-factor	39.65
macromolecules	39.11
solvent	46.88

Table 2.7: Sequence comparisons of enzymes used for molecular replacement and modeling. Sequences were aligned with MAFFT (Katoh and Standley, 2013). Conserved amino acids are indicated by asterisks, similar amino-acids are indicated as colon (PAM 250 score > 0.5) or dots (PAM 250 score ≤ 0.5) at the bottom of each column.

Sequence alignment of *anc*2PabA and *ss*TrpG (seq-identity = 51 %, seq-similarity = 66%, used to generate a template for molecular replacement):

```
anc2PabA        M--ILMIDNYDSFTYNLVQYLGELGEEVVVYRNDEITIAEIEKLKPDHLVISPGPCTP--
ssTrpG          MDLTLIIDNYDSFVYNIAQIVGELGSYPIVIRNDEISIKGIERIDPDRIIISPGPGTPEK
                *   *:*******.**:.* :****.  :* *****:*  **::.**:::***** **

anc2PabA        -NEAGISLEVIKHFAGKIPILGVCLGHQSIGQAFGGKIVRAKQVMHGKTSEIYHNNK---
ssTrpG          REDIGVSLDVIKYLGKRTPILGVCLGHQAIGYAFGAKIRRARKVFHGKISNIILVNNSPL
                 :: *:**:***::. : **********:** ***.** **::*:*** *:*   *:

anc2PabA        GVFKGLNNPFEATRYHSLVVERETLPDCLEITAWTETDEGEIMGIRHKTLPIEGVQFHPE
ssTrpG          SLYYGIAKEFKATRYHSLVVDEVHRP--LIVDAISAEDN-EIMAIHHEEYPIYGVQFHPE
                .:: *: : *:*********:.   *  * : * :  *: ***.*:*:  ** *******

anc2PabA        SILTEQGHELLKNFLKE-
ssTrpG          SVGTSLGYKILYNFLNRV
                *: *. *:::* ***:.
```

Sequence alignment of *ec*PabA and *ss*TrpG (seq-identity = 47%, seq-similarity = 65%, used for homology modeling):

```
ecPabA          M--ILLIDNYDSFTWNLYQYFCELGADVLVKRNDALTLADIDALKPQKIVISPGPCTP--
ssTrpG          MDLTLIIDNYDSFVYNIAQIVGELGSYPIVIRNDEISIKGIERIDPDRIIISPGPGTPEK
                *   *:*******.:*: * . ***:  :* *** ::: .*: :.*::*:***** **

ecPabA          -DEAGISLDVIRHYAGRLPILGVCLGHQAMAQAFGGKVVRAAKVMHGKTSPI---THNGE
ssTrpG          REDIGVSLDVIKYLGKRTPILGVCLGHQAIGYAFGAKIRRARKVFHGKISNIILVNNSPL
                 :: *:*****:: . * ***********:. ***.*: ** **:*** * *   .:.

ecPabA          GVFRGLANPLTVTRYHSLVVEPDSLPACFDVTAWSETREIMGIRHRQWDLEGVQFHPESI
ssTrpG          SLYYGIAKEFKATRYHSLVVDEVHRPLIVDAIS-AEDNEIMAIHHEEYPIYGVQFHPESV
                .:: *:*: :..********:    *  .*. : :* .***.*:*.:: : ********:

ecPabA          LSEQGHQLLANFLHR-
ssTrpG          GTSLGYKILYNFLNRV
                 :. *:::* ***:*
```

Sequence comparison *ec*PabB and *ss*TrpE (seq-identity = 33%, seq-similarity = 53%, used for homology modeling):

```
ecPabB          MKT------LSPAVITLLWRQDAAEFYFSRLSHLPWAMLLHSGYADHPYSRFDIVVAEPI
ssTrpE          MEVHPISEFASPFEVFKCIERD-----------FKVAGLLESIGGPQYKARYSVI-----
                *:.       **  :    .:*           :  * **.*  . :  :*:.::

ecPabB          CTLTTFGKETVVSESEKRTTTTDDPLQVLQQVLDRADIRPTHNEDLP--FQGGALGLFGY
ssTrpE          -AWSTNGYLKI----------HDDPVNILNGYLKDLKL-----ADIPGLFKGGMIGYISY
                 : :* *  .:           ***:::*:  *.  .:      *:*  *:** :* :.*

ecPabB          DLGRRFESLPEI--AEQDIVLPDMAVGIYDWALIVDHQRHTVSLLSHNDVNARRAWLESQ
ssTrpE          DAVRFWEKIRDLKPAAED--WPYAEFFTPDNIIIYDHNEGKVYV--NADLSSVGGCGDIG
                *  * :*.: ::  * :*   *   .   *  :* **:. .* :  : *:.:  .  :

ecPabB          QFSPQEDFTLTSDWQSNMTREQYGEKFRQVQEYLHSGDCYQVNLAQRFHATYSGDEWQAF
ssTrpE          EFK-------VSFYDESLNKNSYERIVSESLEYIRSGYIFQVVLSRFYRYIFSGDPLRIY
                :*.       .* ::..:.::.* . . :  **::**  :** *:: ::  :***  : :

ecPabB          LQLNQANRAPFSAFLRLEQGAILSLSPERFILCDNSEIQTRPIKGTLPRLPDPQEDSKQA
ssTrpE          YNLRRINPSPYMFYLKFDEKYLIGSSPELLFRVQDNIVETYPIAGTRPRGADQEEDLKLE
                 :*.: * :*:  :*::::  ::. *** ::  ::. ::* ** ** ** .* :** *

ecPabB          VKLANSAKDRAENLMIVDLMRNDIGRVAVAGSVKVPELFVVEPFPAVHHLVSTITAQLPE
ssTrpE          LELMNSEKDKAEHLMLVDLARNDLGKVCVPGTVKVPELMYVEKYSHVQHIVSKVIGTLKK
                ::* ** **:**:**:*** ***:*:*.*.*:******: ** :. *:*:**.: . * :

ecPabB          QLHASDLLRAAFPGGSITGAPKVRAMEIIDELEPQRRNAWCGSIGYLSFCGNMDTSITIR
ssTrpE          KYNALNVLSATFPAGTVSGAPKPMAMNIIETLEEYKRGPYAGAVGFISADGNAEFAIAIR
                : :* ::* *:**.*:::****  **:**: **  :*..:.*::*::*  ** : :*:**

ecPabB          TLTAINGQIF-CSAGGGIVADSQEEAEYQETFDKVNRILKQLE-----K
ssTrpE          T-AFLNKELLRIHAGAGIVYDSNPESEYFETEHK----LKALKTAIGVR
                * : :* :::   **.*** **: *:** ** .*    ** *:     :
```

Table 2.8: Oligonucleotides used for cloning and site-directed mutagenesis.

Mutant	Primer-forward	Primer-reverse	Soluble (y/n)
ecPabA_D6A	CGAACTACGATTCT	CTATAAGCAGGATCAT	y
ecPabA_N7A	CGTACGATTCTTTTACC	CATCTATAAGCAGGATC	n
ecPabA_Y8A	GGATTCTTTTACCTGG	GCGTTATCTATAAGCAGG	y
ecPabA_D9A	GTCTTTTACCTGGAAC	GCGTAGTTATCTATAAGC	y
ecPabA_S10A	GTTTACCTGGAACCTC	GCATCGTAGTTATCTATAA	y
ecPabA_F11A	GACCTGGAACCTCTAC	GCAGAATCGTAGTTATCTATA	y
ecPabA_R30A	GAACGATGCGTTGACG	GCCTTAACCAGCACATC	y
ecPabA_D32A	GGCGTTGACGCTGG	GCGTTGCGCTTAACCAG	n
ecPabA_P51A	GGCCCCTGTACGC	CGCTGAGATGACAATTTTTTG	y
ecPabA_G52A	GCCCTGTACGCCAG	GCAGGTGAGATGACAATTTTTTG	n
ecPabA_P53A	CGTGTACGCCAGATGAAG	CGCCAGGTGAGATGACAATT	y
ecPabA_T55A	CGCCAGATGAAGCCGGG	CACAGGGGCCAGGTGA	y
ecPabA_G77A	GTCTGCCTCGGTCATC	CGCAAGAATCGGCAAG	n
ecPabA_V78A	CGTGCCTCGGTCATCAG	CGCCAAGAATCGGCAA	n
ecPabA_G81A	CGCATCAGGCAATGGCG	CGAGGCAGACGCCAAG	n
ecPabA_Q83A	GGCAATGGCGCAGG	GCATGACCGAGGCAGAC	n
ecPabA_M100A	CGCACGGCAAAACCTCG	CGACCTTTGCGGCGC	y
ecPabA_H101A	GGGCAAAACCTCGCCGA	GCCATGACCTTTGCGGC	y
ecPabA_G102A	GAAAACCTCGCCGATTACA	GCGTGCATGACCTTTG	y
ecPabA_K103A	CGACCTCGCCGATTACACAT	CGCCGTGCATGACCTT	y
ecPabA_T104A	CGTCGCCGATTACACATAA	CTTTGCCGTGCATGAC	y
ecPabA_T125A	GCGCTACCATTCGCTG	GCCACGGTAAGTGGATTTG	y
ecPabA_R126A	CGTACCATTCGCTGGTG	CTGTCACGGTAAGTGGAT	y
ecPabA_Y127A	CGCATTCGCTGGTGG	CGCGTGTCACGGTAAGT	y
ecPabA_H128A	CGTCGCTGGTGGTGGA	CGTAGCGTGTCACGGTAAG	y
ecPabA_S129A	CGCTGGTGGTGGAACC	CATGGTAGCGTGTCACGGT	y
ecPabA_L130A	CGGTGGTGGAACCTGAC	CCGAATGGTAGCGTGTCAC	y
ecPabA_G164A	GGTGCAGTTCCATCCAG	GCTTCCAGATCCCACTG	n
ecPabA_V165A	GCAGTTCCATCCAGAAAG	GCACCTTCCAGATCCC	n
ecPabA_Q166A	CGTTCCATCCAGAAAGTAT	CCACACCTTCCAGATC	y
ecPabA_F167A	CGCATCCAGAAAGTATTC	CCTGCACACCTTCCA	n
ecPabA_S171A	CGATTCTTAGCGAACAAG	CTTCTGGATGGAACTG	y
ecPabA_I172A	GCTTAGCGAACAAGGAC	GCACTTTCTGGATGGAAC	y
ecPabB_Y112A	GATCTGGGCCGCCGTT	CGCGCCAAACAACCCCAGTG	y
ecPabB_E119A	GCGTCACTGCCAGAAAT	AAAACGGCGGCCC	y

ecPabB_G207A	GGATTGCTATCAGGTG	GCGCTGTGCAGATATTC	y
ecPabB_D208A	GCGTGCTATCAGGTG	ACCGCTGTGCAGATA	y
ecPabB_V212A	CGAATCTCGCCCAACG	CCTGATAGCAATCACCGC	y
ecPabB_N213A	CTCGCCCAACGTTTTC	CGCCACCTGATAGCAATC	y
ecPabB_G275A	GCTTTAATCGGGCGGGT	GACGCTACCACGCCT	y
ecPabB_T276A	CGCCTTTAATCGGGCG	CGCTACCACGCCTG	y
ecPabB_K298A	GCGGATCGTGCCGAAAAT	CGCTGAGTTCGCCAG	y
ecPabB_R300A	GGCCGAAAATCTGATG	GCATCTTTCGCTGAGTT	y
ecPabB_A301V	GTGGAAAATCTGATGATT	ACGATCTTTCGCTGA	y
ecPabB_E302A	GCGAATCTGATGATTGTCG	GGCACGATCTTTCGC	y
ecPabB_M305A	GCGTAATGATATCGGT	GCTAAATCGACAATCAT	y
ecPabB_D308A	CGTTAATGCGTAATGAT	CGACAATCATCAGATT	y
ecPabB_D308E	GAATTAATGCGTAATGA TATCGGTCG	GACAATCATCAGATTTTCGGCAC	y
ecPabB_L309A	CGATGCGTAATGATATC	CATCGACAATCATCAG	y
ecPabB_R311A	GAATGATATCGGTCGT	GCCATTAAATCGACAAT	y
ecPabB_N312A	GGATATCGGTCGTGTT	GCACGCATTAAATCGAC	y
ecPabB_I367A	GACCGGGGCTCCGAAAG	GCTTTTCCTGGTGGCTCAGC	y
ecPabB_G369A	CGGCTCCGAAAGTACG	CGGTTATTGAGCCACCAG	y
ecPabB_A370V	GTTCCGAAAGTACGGGCT	CCCGGTTATTGAGCC	y
ecPabB_K372A	GCGGTACGGGCTATGGAA	CGGAGCCCCGGTTATT	y
ecPabB_R374A	GGTACGGGCTATGGAAAT	TAACCGGGGCTCCGGC	y
ecPabB_A423V	GGCGGTGGAATTGTC	CACAGAGCAGAAAATTTGTC	y
ecPabB_G424A	GGTGGAATTGTCGCCG	CGCCGCAGAGCAGAAAAT	y
ecPabB_G426A	GCGATTGTCGCCGATAGC	ACCGCCCGCAGAGCA	y
ecPabB_V428A	CGGCCGATAGCCAG	CAATTCCACCGCCCG	y

Table 2.9: Steady-state kinetic parameters for the glutamine-dependent ADCS activity.

Glutaminase	Synthase	K_M^{Gln} [mM]	k_{cat} [s^{-1}]	k_{cat}/K_M^{Gln} [$M^{-1}s^{-1}$]
aD6A	bWT	>5	> 0.01	1.1
aY8A	bWT	7.38 ± 0.76	0.25 ± 0.01	34.4 ± 5.5
aD9A	bWT	0.33 ± 0.15	0.017 ± 0.002	53.5 ± 29.3
aS10A	bWT	1.09 ± 0.32	0.011 ± 0.001	10.7 ± 4.1
aF11A	bWT	1.24 ± 0.29	0.099 ± 0.006	80.1 ± 24.7
aR30A	bWT	6.28 ± 1.30	0.12 ± 0.01	19.0 ± 6.0
aP51A	bWT	1.29 ± 0.15	0.33 ± 0.01	252.9 ± 38.2
aP53A	bWT	0.73 ± 0.06	0.176 ± 0.003	239.9 ± 22.5
aT55A	bWT	1.12 ± 0.18	0.55 ± 0.02	489.2 ± 100.8
aM100A	bWT	0.76 ± 0.09	0.214 ± 0.006	281.6 ± 36.5
aH101A	bWT	n.d.	n.d.	n.d.
aG102A	bWT	1.86 ± 0.14	0.67 ± 0.02	361.3 ± 10.1
aK103A	bWT	0.83 ± 0.10	0.40 ± 0.01	487.3 ± 76.5
aT104A	bWT	0.66 ± 0.05	0.48 ± 0.01	721.7 ± 62.2
aT125A	bWT	0.64 ± 0.04	0.65 ± 0.01	1015.6 ± 79.2
aR126A	bWT	n.d.	n.d.	n.d.
aY127A	bWT	n.d.	n.d.	n.d.
aH128A	bWT	>10	>0.2	19.4
aS129A	bWT	2.63 ± 0.24	0.37 ± 0.01	140.4 ± 17.7
aL130A	bWT	6.79 ± 1.83	0.11 ± 0.02	16.8 ± 6.9
aQ166A	bWT	4.95 ± 1.02	0.18 ± 0.02	36.5 ± 11.1
aS171A	bWT	0.061 ± 0.007	0.058 ± 0.001	963.0 ± 134.5
aI172A	bWT	2.54 ± 0.21	0.41 ± 0.01	161.0 ± 18.0
aWT	bY112A	0.12 ± 0.04	0.047 ± 0.002	396.3 ± 145.2
aWT	bE119A	8.43 ± 1.26	0.51 ± 0.04	60.3 ± 14.2
aWT	bG207A	8.00 ± 2.26	0.13 ± 0.02	16.5 ± 7.3
aWT	bD208A	n.d.	n.d.	n.d.
aWT	bV212A	0.40 ± 0.04	0.27 ± 0.01	682.1 ± 81.5
aWT	bN213A	0.59 ± 0.05	0.367 ± 0.007	624.1 ± 62.4
aWT	bG275A	0.34 ± 0.19	0.013 ± 0.001	37.2 ± 24.9
aWT	bT276A	0.11 ± 0.05	0.138 ± 0.001	235.3 ± 106.7
aWT	bK298A	n.d.	n.d.	n.d.
aWT	bR300A	0.41 ± 0.06	0.31 ± 0.01	765.9 ± 124.3
aWT	bA301V	1.99 ± 0.11	0.51 ± 0.01	253.3 ± 18.3
aWT	bE302A	n.d.	n.d.	n.d.
aWT	bM305A	0.51 ± 0.06	0.298 ± 0.007	580.9 ± 78.7

aWT	bD308A	n.d.	n.d.	n.d.
aWT	bD308E	0.38 ± 0.10	0.10 ± 0.01	261.0 ± 82.5
aWT	bL309A	n.d.	n.d.	n.d.
aWT	bR311A	3.41 ± 0.75	0.037 ± 0.003	10.9 ± 3.4
aWT	bN312A	0.42 ± 0.04	0.103 ± 0.002	246.9 ± 25.4
aWT	bI367A	0.52 ± 0.18	0.031 ± 0.002	59.1 ± 25.5
aWT	bG369A	n.d.	n.d.	n.d.
aWT	bA370V	1.01 ± 0.05	0.208 ± 0.003	207.1 ± 12.4
aWT	bR374A	0.54 ± 0.12	0.20 ± 0.01	383.3 ± 101.7
aWT	bA423V	0.26 ± 0.02	0.483 ± 0.006	1888.3 ± 150.5
aWT	bG424A	0.35 ± 0.07	0.041 ± 0.002	134.7 ± 30.8
aWT	bG426A	0.45 ± 0.04	0.38 ± 0.01	851.5 ± 101.6
aWT	bV428A	0.12 ± 0.06	0.019 ± 0.002	154.9 ± 93.1
aWT	bWT	0.37 ± 0.03	0.55 ± 0.01	1464.6 ± 158.3

n.d. = not detectable

Table 2.10: Amino acid sequences of *anc1-3*PabA

>*anc*1PabA
MILMIDNYDSFTYNLVQYLGELGEEVVVKRNDEITIAEIEQLKPDFLVISPGPCTPNEAGI
SLEVIKHFAGKIPIFGVCLGHQSIAQVFGGEVVRAERLMHGKTSPIFHDGKGIFAGLPNP
FTATRYHSLIVKRETLPDCLEVTAWTEEGEIMGIRHKTLPIEGVQFHPESILTEHGHELL
KNFITLYRKK
>*anc*2PabA
MILMIDNYDSFTYNLVQYLGELGEEVVVYRNDEITIAEIEKLKPDHLVISPGPCTPNEAG
ISLEVIKHFAGKIPILGVCLGHQSIGQAFGGKIVRAKQVMHGKTSEIYHNNKGVFKGLNN
PFEATRYHSLVVERETLPDCLEITAWTETDEGEIMGIRHKTLPIEGVQFHPESILTEQGH
ELLKNFLKE
>*anc*3PabA
MLLMIDNYDSFTYNLVQYLGELGEDVCVYRNDEITIAEIEALRPDHLVISPGPCTPNEAG
ISLAVIRHFAGKIPILGVCLGHQSIGQAFGGRIVRAKQVMHGKTSQVYHNNKGVFAGLN
NPFEATRYHSLVIERETLPDCLEITAWTETDTGELDEIMGIRHKTLPIEGVQFHPESILTE
QGHDLLRNFLKQ

Table 2.11: Amino acid sequences of *E. coli* aminodeoxychorismate synthase

>ecPabA_WT - Accession Number WP_000601847
MILLIDNYDSFTWNLYQYFCELGADVLVKRNDALTLADIDALKPQKIVISPGPCTPDEA
GISLDVIRHYAGRLPILGVCLGHQAMAQAFGGKVVRAAKVMHGKTSPITHNGEGVFRG
LANPLTVTRYHSLVVEPDSLPACFDVTAWSETREIMGIRHRQWDLEGVQFHPESILSEQ
GHQLLANFLHR

>ecPabB_WT - Accession Number WP_000854958
MKTLSPAVITLLWRQDAAEFYFSRLSHLPWAMLLHSGYADHPYSRFDIVVAEPICTLTT
FGKETVVSESEKRTTTTDDPLQVLQQVLDRADIRPTHNEDLPFQGGALGLFGYDLGRR
FESLPEIAEQDIVLPDMAVGIYDWALIVDHQRHTVSLLSHNDVNARRAWLESQQFSPQE
DFTLTSDWQSNMTREQYGEKFRQVQEYLHSGDCYQVNLAQRFHATYSGDEWQAFLQ
LNQANRAPFSAFLRLEQGAILSLSPERFILCDNSEIQTRPIKGTLPRLPDPQEDSKQAVKL
ANSAKDRAENLMIVDLMRNDIGRVAVAGSVKVPELFVVEPFPAVHHLVSTITAQLPEQL
HASDLLRAAFPGGSITGAPKVRAMEIIDELEPQRRNAWCGSIGYLSFCGNMDTSITIRTL
TAINGQIFCSAGGGIVADSQEEAEYQETFDKVNRILKQLEK

Chapter 3

A Fold-Independent Interface Residue Is Crucial for Complex Formation and Allosteric Signaling in Class I Glutamine Amidotransferases

3.1 Abstract

The members of the glutamine amidotransferase (GATase) family catalyze the incorporation of ammonia within numerous metabolic pathways and can be categorized in two classes. Here, we concentrated on class I GATases, which are heteromeric enzyme complexes consisting of synthase subunits and glutaminase subunits with a catalytic Cys-His-Glu triad. Glutamine hydrolysis at the glutaminase subunit is (i) dependent on the formation of tight synthase−glutaminase complexes and (ii) allosterically coupled to the presence of the substrate at the synthase subunit. The structural basis of both complex formation and allostery is poorly understood. However, previous work on 4-amino-4-deoxychorismate synthase and imidazole glycerol phosphate synthase suggested that a conserved aspartate residue in their synthase subunits, which is located at the subunit interface close to the glutaminase catalytic triad, might be important for both features. We performed a computational screen of class I GATases from the Protein Data Bank and identified conserved and similarly located aspartate residues. We then generated alanine and glutamate mutants of these residues and characterized them by analytical gel filtration and steady-state enzyme kinetics. The results confirmed the important role of the wild-type aspartate residues for the formation of stable synthase−glutaminase complexes (in three of four cases) and the stimulation of glutaminase activity in the analyzed GATases (in all four cases). We present a model for rationalizing the dual role of the conserved aspartate residue toward a unifying regulation mechanism in the entire class I GATase family.

3.2 Introduction, Results, and Discussion

The enzymatic incorporation of ammonia into key metabolites is of central physiological importance in bacteria. Most enzymes that catalyze this incorporation belong to the family of

glutamine amidotransferases (GATases) (Mouilleron and Golinelli-Pimpaneau, 2007; Raushel et al., 1999; Zalkin and Smith, 1998). GATases are heteromeric enzyme complexes consisting of a glutaminase and a synthase subunit. The glutaminase subunit hydrolyzes glutamine to glutamate and ammonia, which is incorporated into the substrate of the synthase subunits (Massiere and Badet-Denisot, 1998). GATases have evolved sophisticated coupling mechanisms between their subunits. First, they form tight synthase−glutaminase complexes, in which both active sites are connected via a channel that shields the reactive ammonia from solvent to prevent its unproductive loss by diffusion and solvent protonation (Zalkin and Smith, 1998; Oliver et al., 2014; Raushel et al., 2003). Second, an allosteric mechanism, which couples glutaminase activity to the presence of the substrate at the synthase, prevents unproductive hydrolysis of glutamine (Amaro et al., 2007; Chaudhuri et al., 2003).

Whereas the synthases belong to several, structurally unrelated protein families, the glutaminases can be categorized into those possessing a Cys-His-Glu catalytic triad and an α/β hydrolase fold (class I) or those of the Ntn type (class II) characterized by an N-terminal catalytic cysteine residue. While conformational changes underlying allosteric coupling of synthase and glutaminase subunits have been well characterized for glucosamine-6-phosphate synthase (Mouilleron et al., 2011), a prominent member of the class II GATases, less is known in this respect about class I GATases. Because of the structural diversity in the synthases of class I GATases (Douangamath et al., 2002; Morollo and Eck, 2001; Thoden et al., 1998; Parsons et al., 2002; Li et al., 2011), it has been difficult to identify a general allosteric mechanism. Thus, the molecular details of glutaminase activation are only poorly understood.

We recently analyzed the allosteric communication pathways within 4-amino-4-deoxychorismate synthase (ADCS) (Semmelmann et al., 2019), a member of class I GATases. We identified four conserved allosteric signaling pathways that lead to activity-inducing conformational changes at the glutaminase subunit PabA as a consequence of the binding of the substrate chorismate to the synthase subunit PabB. Interestingly, we identified a conserved aspartate residue of PabB (D308 in the enzyme from *E. coli*) at the synthase−glutaminase interface in the proximity of the glutaminase active site as the key residue for both complex formation and allosteric signaling. As part of a broad intersubunit hydrogen-bond network (Semmelmann et al., 2019), this aspartate residue forms two polar contacts to (i) an interaction hot-spot residue (Y127) and (ii) an allosteric residue (S171) of the glutaminase subunit. Mutation of this aspartate residue to alanine resulted in a drastic reduction of glutaminase activity that accompanied the loss of formation of a stable synthase−glutaminase complex most likely caused by disruption of the D308−Y127 hydrogen bond. In contrast, the introduction of a glutamate residue at this position led to increased glutaminase activity, most likely caused by spatial changes of the D308−S171 hydrogen bond. We concluded that the longer side chain of glutamate might mimic a potential movement of the wild-type aspartate side chain toward the glutaminase active site during allosteric signaling. Strikingly, the comparison with imidazole glycerol phosphate synthase (ImGPS), another reasonably well characterized class I GATase (Rivalta et al., 2012, 2016; List et al., 2012b;

Myers et al., 2005), revealed that there is also a conserved, allosterically important aspartate residue (D98 in the enzyme from *Thermotoga maritima*) in the synthase subunit located at the analogous position of the synthase−glutaminase interface (List et al., 2012b). The central importance of these aspartate residues in ADCS and ImGPS along with the fact that both synthases possess different folds [four-layer sandwich fold for ADCS (Parsons et al., 2002) and $(\beta/\alpha)_8$-barrel fold for ImGPS (Douangamath et al., 2002)] led us to hypothesize the existence of a fold-independent mechanism of catalytic coupling in class I GATases. More specifically, we presumed that in class I GATases, a coupling donor Asp residue in the synthase (abbreviated as d-Asp-s in the following) and at least one glutaminase-specific acceptor residue (abbreviated as a-Res-g in the following) near the catalytic His of the glutaminase subunit (abbreviated as c-His-g in the following) are linked by a polar interaction that is crucial for (i) complex formation and/or (ii) transfer of the allosteric signal to the catalytic triad of class I GATases. To test this hypothesis, we scanned the Protein Data Bank (PDB) for class I GATases possessing a d-Asp-s residue linked by polar interactions to corresponding a-Res-g residues in the vicinity of c-His-g (Figure 3.1A). We found such donor/acceptor residue combinations in 33 crystal structures of class I GATase complexes, including anthranilate synthase (AS), 2-amino-2-deoxyisochorismate synthase (PhzE), formylglycinamide ribonucleotide synthetase (FGARS), carbamoylphosphate synthetase (CPS), and ImGPS, along with our query structure ADCS (Figure 3.1B and Table 3.2). We did not detect d-Asp-s residues in the remaining class I GATases CTP synthetase, pyridoxal 5′-phosphate synthetase, and GMP synthetase for reasons described in the Supporting Information (Experimental Procedures).

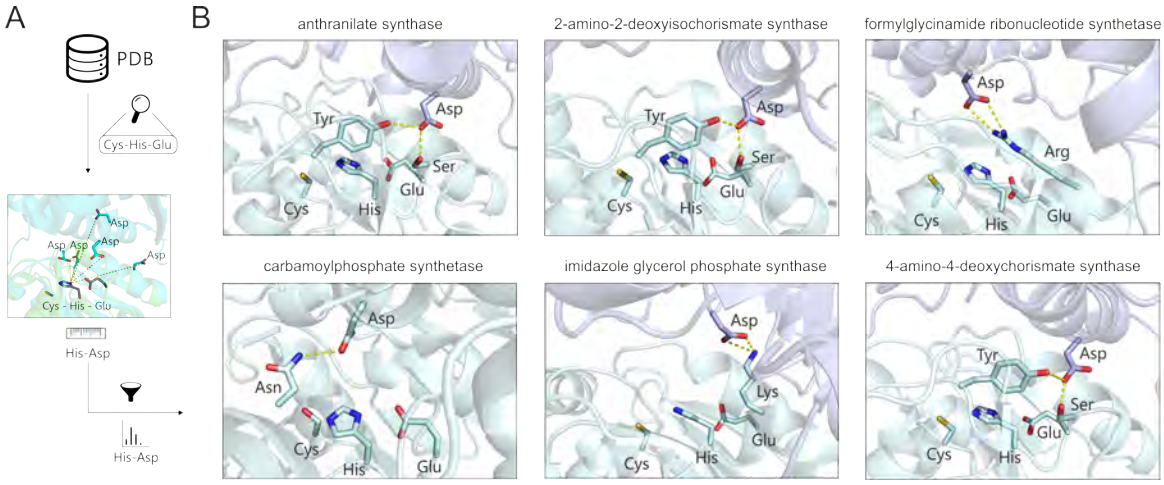

Figure 3.1: Identification of d-Asp-s residues forming polar interactions with a-Res-g residues in the vicinity of c-His-g. (A) By superposition (TM-align (Zhang and Skolnick, 2005) cutoff of 0.5) with a model of *E. coli* PabA (green), all PDB entries that had a class I GATase glutaminase fold were identified. The existence of a catalytic triad (Cys-His-Glu) was confirmed by visual inspection. For all putative d-Asp-s residues (maximal distance of 15 Å from a c-His-g residue), the existence of polar interactions with an a-Res-g residue was examined. In 33 structures, a d-Asp-s residue that featured at least one polar interaction with an a-Res-g in the vicinity of c-His-g was identified (Table S1). (B) GATases possessing a d-Asp-s interacting with an a-Res-g in the glutaminase active site. Catalytic and interacting residues are shown as sticks, and interactions are shown as yellow dashes.

To test the structural role of the d-Asp-s residues, we paradigmatically generated, purified, and characterized by analytical size exclusion chromatography wild-type as well as alanine and glutamate mutants of the d-Asp-s residues in AS, PhzE, ImGPS, and ADCS (Figure 3.2).

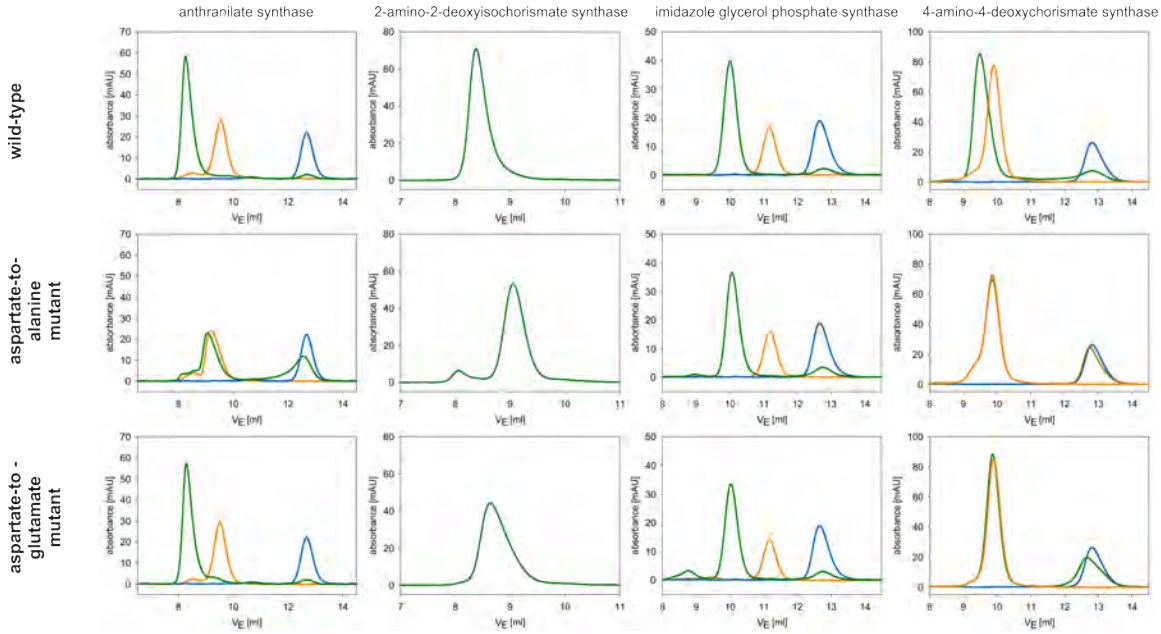

Figure 3.2: Analytical size exclusion chromatography with wild-type and d-Asp-s mutant GATases. The proteins (50 µM, subunit concentration) were applied to a S75 analytical column equilibrated with 50 mM Tris (pH 7.5), 150 mM KCl, and 5 mM $MgCl_2$. Elution was performed at a flow rate of 0.5 mL/min and followed by measuring the absorption at 280 nm, which was plotted against the elution volume (V_E). The identity of the enzymes is indicated at the top, and the wild-type or mutants are indicated on the left. Data for single-glutaminase subunit runs are colored blue, data for single-synthase subunit runs orange, and data for complex runs of synthase and glutaminase green. For 2-amino-2-deoxyisochorismate synthase, where the glutaminase and synthase subunits are organized as a fusion protein that forms intertwined homodimers, data for the single runs are colored green.

The wild-type enzymes formed the expected stable synthase−glutaminase complexes (Figure 3.2, top panels). Strikingly, whereas the aspartate-to-alanine mutant of ImGPS eluted like the wild-type enzyme, the corresponding mutants of AS, PhzE, and ADCS were unable to form complexes (Figure 3.2, middle panels). This result was somewhat unexpected for PhzE, where the aspartate-to-alanine mutation led to disruption of the intertwined homodimer (two protomers each consisting of a glutaminase and a synthase domain; the glutaminase domain of one protomer interacting with the synthase domain of the other protomer) to the monomer (one protomer consisting of a glutaminase and a synthase domain). In contrast, the aspartate-to-glutamate mutants of AS and ImGPS still formed stable complexes and the corresponding PhzE mutant eluted at slightly larger volumes compared to the wild-type enzyme, indicating a fast equilibrium between complexed and noncomplexed subunits (Figure 3.2, bottom panels). The aspartate-to-glutamate mutant of ADCS was no longer able to form a stable complex.
To test the functional role of the d-Asp-s residues, we performed steady-state kinetics of glutaminase activity for wild-type and mutant enzymes (Table 3.1).

Table 3.1: Steady-State Glutaminase Activity Kinetics of Wild-Type and d-Asp-s Mutant GATases

	without an allosteric effector			with an allosteric effector		
	K_M^{Gln} (mM)	k_{cat} (s^{-1})	k_{cat}/K_M^{Gln} (M^{-1} s^{-1})	K_M^{Gln} (mM)	k_{cat} (s^{-1})	k_{cat}/K_M^{Gln} (M^{-1} s^{-1})
Glutaminase Activity of Anthranilate Synthase (AS)[a]						
wild type	1.26 ± 0.27	0.16 ± 0.01	(1.29 ± 0.36) × 10^2	0.23 ± 0.07	0.93 ± 0.19	(4.09 ± 2.18) × 10^3
D367A	>10	>0.08	8.0	2.94 ± 0.20	0.24 ± 0.03	(8.02 ± 1.54) × 10
D367E	>10	>0.25	25.4	0.126 ± 0.003	0.381 ± 0.004	(3.04 ± 0.09) × 10^3
Glutaminase Activity of 2-Amino-2-deoxyisochorismate Synthase (PhzE)[a]						
wild type	3.63 ± 0.06	1.04 ± 0.16	(2.87 ± 0.49) × 10^2	0.16 ± 0.01	0.62 ± 0.03	(3.73 ± 0.32) × 10^3
D250A	>10	>0.25	24.3	>10	>0.01	1.4
D250E	>10	>0.15	14.6	1.98 ± 0.11	0.40 ± 0.01	(2.02 ± 0.15) × 10^2
Glutaminase Activity of Imidazole Glycerol Phosphate Synthase (ImGPS)[b]						
wild type	2.46 ± 0.91	(2.83 ± 0.01) × 10^{-5}	(1.15 ± 0.37) × 10^{-2}	0.64 ± 0.08	(8.79 ± 0.31) × 10^{-2}	(1.37 ± 0.12) × 10^2
D98A	–	<1 × 10^{-7}	–	–	<1 × 10^{-7}	–
D98E	4.18 ± 1.38	(2.92 ± 0.01) × 10^{-4}	(7.00 ± 2.33) × 10^{-2}	0.24 ± 0.02	0.41 ± 0.01	(1.70 ± 0.09) × 10^3
Glutaminase Activity of 4-Amino-4-deoxychorismate Synthase (ADCS)[a]						
wild type	0.18 ± 0.03	0.26 ± 0.05	(1.47 ± 0.58) × 10^3	0.31 ± 0.02	0.52 ± 0.03	(1.68 ± 0.23) × 10^3
D308A	>10	>0.05	5.0	>10	>0.09	9.0
D308E	0.43 ± 0.03	0.333 ± 0.003	(7.70 ± 0.61) × 10^2	0.231 ± 0.005	0.35 ± 0.09	(1.51 ± 0.43) × 10^3

[a]Reaction conditions: 50 mM Tricine-KOH (pH 8.0), 150 mM KCl, 0.5−1 μM glutaminase, 1.5−3 μM synthase, 0.01−10 mM L-glutamine, 0 or 100 μM chorismate. [b]Reaction conditions: 20 mM Tris-HCl (pH 7.0), 0.05 μM glutaminase, 0.05−10 mM L-glutamine, 0 or 70 μM ProFAR.

For the wild-type enzymes, we observed the expected allosteric stimulation of glutaminase activity by the presence of the substrate at the synthase subunit. The turnover number (k_{cat}) was enhanced between ∼2-fold (ADCS) and ∼3000-fold (ImGPS). Moreover, with the exception of ADCS, the Michaelis constant (K_M^{Gln}) was slightly decreased. In accordance with the lost ability to form stable complexes (Figure 3.2), the alanine mutants of AS, PhzE, and ADCS showed drastically impaired glutaminase activity, irrespective of the presence of the substrate at the synthase subunit. Strikingly, for the alanine mutant of ImGPS, no glutaminase activity was detectable, indicating that the deactivating effect might be entirely caused by allosteric effects. For the glutamate mutants, we observed different effects on catalytic parameters. Whereas in ADCS, k_{cat} and K_M^{Gln} are comparable in the absence or presence of the synthase substrate, for AS and PhzE the glutamate mutants displayed drastically impaired catalytic activities but were activated upon binding of the synthase substrate. For ImGPS, the k_{cat} of the glutamate mutant was, surprisingly, significantly higher than that for the wild-type enzyme and further stimulated ∼1000-fold in the presence of the synthase substrate.

Despite the structural diversity observed in class I GATases, our study demonstrates that single aspartate residues within the synthase subunits of AS, PhzE, ImGPS, and ADCS are crucial for complex formation and allosteric coupling between their synthase and glutaminase subunits. As for complex formation, we found that enzymes whose d-Asp-s alanine mutants were not able to form stable synthase−glutaminase complexes (AS, PhzE, and ADCS) possess the a-Res-g residue tyrosine (Figure 3.1B). Analogously to ADCS, where the alanine mutant of this tyrosine residue has been characterized (Semmelmann et al., 2019), we conclude that the hydrogen bond between d-Asp-s and a-Res-g tyrosine is crucial for complex formation in these enzymes.

As for allosteric signaling, in 33 crystal structures of AS, PhzE, FGARS, ImGPS, and ADCS, from different organisms (Table 3.2), the d-Asp-s residues additionally interact with a-Res-g

residues that are located three positions downstream of c-His-g (HPE-S in AS and ADCS, HAE-S in PhzE, HPE-R in FGARS, and HPE-K in ImGPS) in highly conserved regions of the enzymes (Figure 3.3). The chemical nature of the a-Res-g residues might thereby determine the strictness of allosteric coupling. Whereas the longer side chain of lysine in ImGPS results in the strictest allosteric coupling observed (∼3000-fold activation for the wild-type enzyme), the shorter side chains of serine in AS, PhzE, and ADCS lead to a looser coupling (∼2−10-fold activation). Previous studies of yeast ImGPS suggested that the interaction between its d-Asp-s residue (D383) and its a-Res-g residue (K196) pulls the glutaminase loop (HPE-K) containing c-His-g (H193) away from the catalytic cysteine. As a consequence, in the absence of the synthase substrate, H193 would be prevented from functioning in the catalytic cycle (Myers et al., 2005). In the presence of the synthase substrate, relief of the D383−K196 interaction might allow H193 to move toward the catalytic cysteine, resulting in glutamine turnover (Myers et al., 2005). The shorter a-Res-g serine residues of the glutaminase subunits in AS, PhzE, and ADCS might be less efficient in pulling the c-His-g away from the catalytic cysteine, and therefore, the allosteric coupling would be less strict for these enzymes.

From an evolutionary perspective, the coalition of complex formation and allosteric signaling in a single aspartate residue seems feasible and efficient. Instead of imposing these important physiological functionalities upon two or more different residues in the protein−protein interface, the aspartate residues described here seem to serve as anchors for the interaction and allosteric coupling between synthase and glutaminase subunits. This anchor might ultimately have allowed for the accumulation of mutations within the protein−protein interface of class I GATases that are responsible for the delicate interaction specificities we observe today for this ubiquitous family of enzymes (Plach et al., 2017).

ASSOCIATED CONTENT

Supporting Information

The Supporting Information is available free of charge on the ACS Publications website at DOI: 10.1021/acs.biochem.9b00286. Experimental procedures (PDF)

Accession Codes

WP_011355173, WP_001194371 , ELN96503, WP_000601847, WP_000854958, WP_004080484.1, WP_004080486.1.

AUTHOR INFORMATION

Corresponding Author

*E-mail: Reinhard.Sterner@ur.de.

ORCID

Reinhard Sterner: 0000-0001-8177-8460

Author Contributions

F.S. designed experiments. F.S. and E.H. performed and analyzed experiments. F.S. and L.H. performed computations. F.S., R.M., and R.S. wrote the manuscript with contributions from E.H. and L.H.

Funding

F.S. was supported by a doctoral fellowship from the Konrad-Adenauer-Stiftung.

Notes

The authors declare no competing financial interest.

ACKNOWLEDGMENTS

The authors thank Jeannette Ueckert for expert technical assistance.

3.3 Supporting Information

3.3.1 Experimental Procedures

Cloning and Mutagenesis

The genes of ADCS (*ec*PabA and *ec*PabB), AS (*st*TrpG and *st*TrpE) and the genes of ImGPS (*tm*HisH and *tm*HisF) were available cloned into the pET21a expression plasmid from previous studies (Plach et al., 2017; List et al., 2012b). The gene for PhzE was synthesized (Life Technologies) and cloned into the pET28a_*Bsa*I expression plasmid as described (Rohweder et al., 2018). Single amino acid mutant enzymes were produced using a modified QuickChange mutagenesis protocol (Wang and Malcolm, 1999) with the primers listed in Table 3.3. The amino acid sequences of analyzed wild-type proteins and their accession numbers are listed in Table 3.4.

Expression and Purification of Proteins

Glutaminase and synthase subunits of *E. coli* ADCS (*ec*PabA, *ec*PabB), *S. typhimurium* AS (*st*TrpG, *st*TrpE) and *T. maritima* ImGPS (*tm*HisH, *tm*HisF) and mutants thereof were produced and purified as previously described (Plach et al., 2017; List et al., 2012b). All other proteins were produced by gene expression in *E. coli* BL21-Gold (DE3) cells. Overnight cultures of individual clones were used to inoculate 2 L of Luria broth medium supplemented with 150 µg/mL kanamycin. Cells were grown at 37 °C to an OD_{600} of 0.6 and then cooled to 25 °C. Expression was induced by adding 0.5 mM isopropyl β-D-1-thiogalactopyranoside and growth was continued overnight at 20 °C. Cells were harvested by centrifugation (2700 g, 4 °C), resuspended in 50 mM Tris-HCl, pH 7.5, 300 mM KCl, 10 mM imidazole, and lyzed by sonification. The insoluble fraction was removed by centrifugation (23000 g, 4 °C) and the soluble extracts were filtered through a 0.8 µm membrane. Supernatants containing the C-terminal hexahistidine-tagged proteins were loaded onto a HisTrapFF crude column (5 mL, GE Healthcare), which had been equilibrated with resuspension buffer, and eluted from the column by applying a linear gradient of 10 - 750 mM imidazole. Enzyme-containing fractions, as judged by SDS-PAGE, were pooled and further purified by preparative gel filtration (Superdex 75 HiLoad 26/60, 320 mL, GE Healthcare, 50 mM Tris-HCl, pH 7.5, 50 mM KCl, 5 mM $MgCl_2$, 2 mM DTT, 4 °C). Elution fractions were analyzed by SDS-PAGE and the fractions containing pure protein were pooled. The enzymes were finally concentrated to 50-150 µM and flash frozen in liquid nitrogen. Protein concentrations were determined by measuring the absorbance at 280 nm, using the molar extinction coefficient calculated via ExPASy ProtParam (http://web.expasy.org/protparam/).

Identification of d-Asp-s Residues

As part of a custom Python script, TM-align (Zhang and Skolnick, 2005) was used with the cut-off 0.5 and our 3D model of the *E. coli* ADCS glutaminase (*ec*PabA) (Semmelmann et al., 2019) as query to identify class I GATases in the PDB; the existence of a catalytic triad (Cys-His-Glu) was confirmed by visual inspection. To detect all putative candidates, aspartate residues within 15 Å of catalytic histidine residues (c-His-g) were chosen and by using PyMol (Schrödinger, 2018) integrated into a Python script, the distances of their carboxyl-moieties to N1 of the c-His-g residues were determined. Utilizing PyMol functionality, those aspartate residues that possessed at least one polar contact to an acceptor residue of the glutaminase active site were selected as d-Asp-s residues.

We were unable to detect d-Asp-s residues in the class I glutamine amidotransferases of guanosine monophosphate synthetase (GMPS), cytidine triphosphate synthetase (CTPS), and pyridoxal 5'-phosphate synthase (Pdx1:Pdx2) for reasons described below.

In GMPS, glutaminase and synthase domain are exposed to solvent and widely separated from one another, suggesting that substantial movement between these domains has to occur in order to couple their catalytic reactions (Tesmer et al., 1996). However, for GMPS the interaction of a synthase domain glutamate residue and a glutaminase domain histidine residue (E383 and H186 for the enzyme from *E. coli*) was shown to be essential for allosteric coupling (Oliver et al., 2014).

For CTPS, it was previously proposed that a synthase domain histidine residue and its interaction with a glutaminase domain serine residue (H314 and S520 for the enzyme from the *E. coli*) might be involved in allosteric signaling (Myers et al., 2005).

For Pdx1:Pdx2, there is no evidence for allosteric communication between its Pdx2 glutaminase subunit and its Pdx1 synthase subunit. It was shown that activation of Pdx1 by Pdx2 was solely caused by proper formation of the oxyanion hole motif in response to complex formation (Strohmeier et al., 2006) and that no further allosteric stimulation occurred (Raschle et al., 2005).

Computation of Amino Acid Conservation and Sequence Logos

410 sequences for ADCS (PabA and PabB) (Plach et al., 2017), 285 sequences for AS (TrpG and TrpE) (Plach et al., 2017), and 1308 sequences for ImGPS (HisH and HisF) (Holinski et al., 2017) were available from previous studies. Sequences for PhzE were extracted from the nr database by using blastp (Altschul et al., 1997) with the *bl*PhzE sequence as query and an e-value cutoff 1E-60. Applying the 90% redundancy filter of Jalview (Waterhouse et al., 2009) reduced the number of hits to 54; these sequences were aligned with MAFFT (Katoh and Standley, 2013). The resulting MSA served as input for WebLogo (Crooks et al., 2004) to compute a sequence logo with a color code representing the chemical properties of the residues: purple, amido; red, acidic; blue, basic; black, hydrophobic; green, hydroxyl functionality and glycine.

Analysis of Complex Formation Between Different Synthases and Glutaminases

The ability to form heteromeric complexes was examined by size exclusion chromatography (SEC) as previously described (Semmelmann et al., 2019). In brief, the experimental setup of SEC comprised a Superdex 75 10/300 GL column (GE Healthcare) operated on an ÄKTAmicro system (GE Healthcare) connected to an ALIAS autosampler (Spark Holland). The system was operated at 25 °C with a flow-rate of 0.5 mL/min of degassed buffer (50 mM Tris-HCl pH 7.5, 150 mM KCl, 5 mM $MgCl_2$) and was calibrated with conalbumin, ovalbumin, carbonic anhydrase, ribonuclease A, and aprotinin from the GE Healthcare SEC low-molecular-weight as well as the SEC high-molecular-weight calibration kit. Individual synthases and glutaminases were assayed at a concentration of 50 µM (applied volume 50 µL). For analysis of complex formation, synthases and glutaminases were equimolarly mixed to a final concentration of 50 µM.

Steady-State Enzyme Kinetics

For ADCS, AS, and PhzE the glutaminase activity was measured spectrophotometrically in a coupled enzymatic assay. Glutamate formed by the glutaminases was converted to α-ketoglutarate by glutamate-dehydrogenase (GDH) with simultaneous reduction of NAD^+ to NADH. A standard assay contained 50 mM tricine-KOH buffer, pH 8.0, 150 mM KCl, 5 mM $MgCl_2$, 1 mM DTT, 10 mM NAD^+, 1 mg/mL GDH, 0 (- allosteric effector) or 100 µM (+ allosteric effector) chorismate and 0.5 µM glutaminase and 1.5 µM synthase. Following preincubation, 0.01-10 mM glutamine was added and the reaction was monitored at 340 nm and 25 °C. The slopes of the linear parts of the progress curves were fitted to the Michaelis-Menten equation with a custom python script.
For ImGPS, the glutaminase activity was measured in a coupled assay using the oxidation of glutamate to α-ketoglutarate, ammonia and hydrogenperoxide by glutamate oxidase (GOX). H_2O_2 was reduced by horseradish peroxidase (HRP), using 4-amino antipyrine (AAP) and phenol as final electron acceptors to yield a quinoide chromophore. A standard assay contained 20 mM Tris/HCl pH 7.0, 1 mM AAP, 1 mM phenol, 20 mU/ml GOX, 1 U/ml HRP, 0 (- allosteric effector) or 70 µM ProFAR (+ allosteric effector), 36 µM (- allosteric effector) or 1 (+ allosteric effector) synthase and 0-10 mM glutamine. After a 1 h preincubation, the reaction was started by addition of 0.05 µM (with ProFAR) of 35 µM (without ProFAR) glutaminase. The reaction progress was monitored by the absorbance at 505 nm at 25 °C. The slopes of the linear parts of the progress curves were fitted to the Michaelis-Menten equation.

3.3.2 Supplementary Figure and Tables

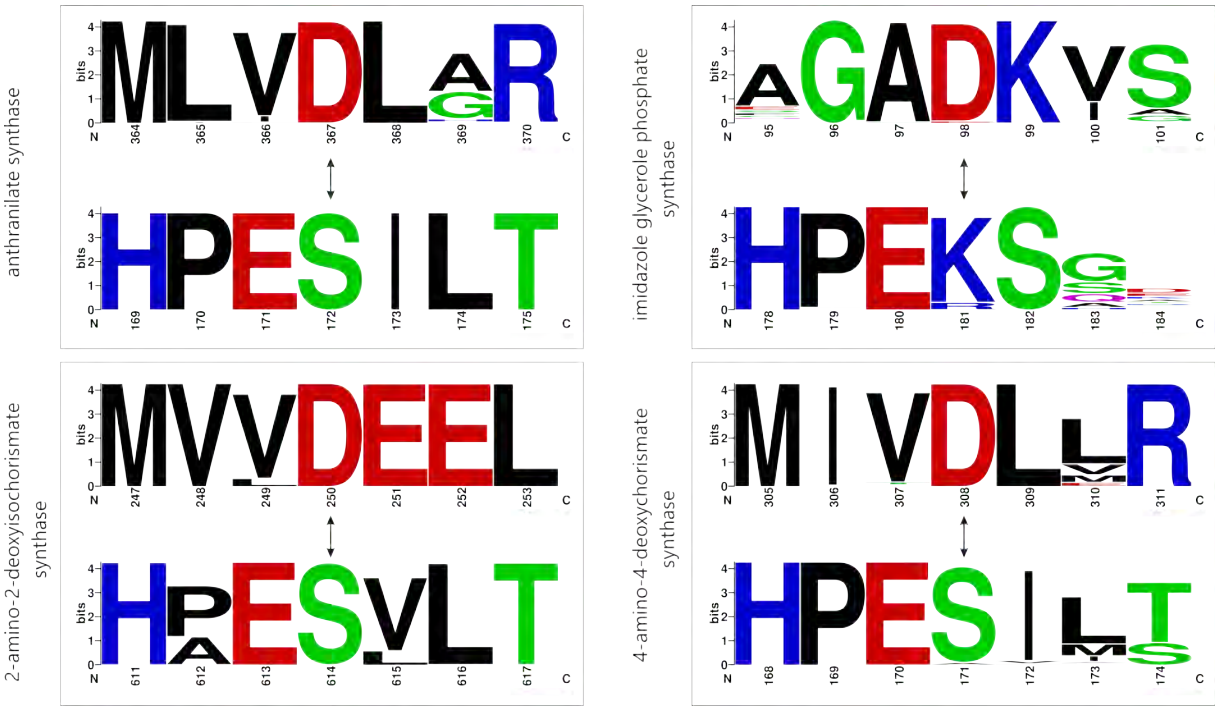

Figure 3.3: Sequence Logos of Experimentally Characterized Class I GATases.

Table 3.2: Overview of Identified d-Asp-s and a-Res-g Residues in Class I GATases.

PDB-ID	Enzyme	Organism	d-Asp-s	a-Res-g
n.a.	ADCS	*Escherichia coli* K12	D308	Y127, S171
3R74	PhzE	*Burkholderia lata* 383	D250	Y566, S614
3R75	PhzE	*Burkholderia lata* 383	D250	Y566, S614
3R76	PhzE	*Burkholderia lata* 383	D250	Y566, S614
1I7Q	AS	*Serratia marcescens*	D367	Y133, S175
1I1Q	AS	*Salmonella typhimurium* strain LT2	D367	Y131, S172
1I7S	AS	*Serratia marcescens*	D367	Y133, S175
1QDL	AS	*Sulfolobus solfataricus*	D275	Y135, S178
1KEE	CPS	*Escherichia coli* K12	D45/D258	N311/G359
1JDB	CPS	*Escherichia coli* K12	D45/D258	N311/G359
1T36	CPS	*Escherichia coli* K12	D45/D258	N311/G359
1M6V	CPS	*Escherichia coli* K12	D45/D258	N311/G359
1CE8	CPS	*Escherichia coli* K12	D45/D258	N311/G359
1C30	CPS	*Escherichia coli* K12	D45/D258	N311/G359
1BXR	CPS	*Escherichia coli* K12	D45/D258	N311/G359
1CS0	CPS	*Escherichia coli* K12	D45/D258	N311/G359
3D54	FGARS	*Thermotoga maritima* strain ATCC 43589	D374	R189
3UJN	FGARS	*Salmonella typhimurium* strain LT2	D657	R1263
3UMM	FGARS	*Salmonella typhimurium* strain LT2	D657	R1263
3UGJ	FGARS	*Salmonella typhimurium* strain LT2	D657	T659, R1263
4MGH	FGARS	*Salmonella typhimurium* strain LT2	D657	T659, R1263
4R7G	FGARS	*Salmonella typhimurium* strain LT2	D657	T659, R1263
1T3T	FGARS	*Salmonella typhimurium* strain LT2	D657	T659, R1263
4I78	FGARS	*Salmonella typhimurium* strain LT2	D657	T659, R1263
4LGY	FGARS	*Salmonella typhimurium* strain LT2	D657	T659, R1263
1GPW	ImGPS	*Thermotoga maritima* strain ATCC 43589	D98	K181
1KA9	ImGPS	*Thermus thermophilus* strain ATCC 27634	D99	K181
3ZR4	ImGPS	*Thermotoga maritima* strain ATCC 43589	D98	K181
2WJZ	ImGPS	*Thermotoga maritima* strain ATCC 43589	D98	K181
10X5	ImGPS	*Saccharomyces cerevisiae* strain ATCC 204508	D359	N13, K196
1KA9	ImGPS	*Thermus thermophilus* strain ATCC 27634	D99	K181
1JVN	ImGPS	*Saccharomyces cerevisiae* strain ATCC 204508	D359	N13, K196
10X4	ImGPS	*Saccharomyces cerevisiae* strain ATCC 204508	D359	N13, K196

n.a. = not available
ADCS = 4-amino-4-deoxychorismate synthase
AS = anthranilate synthase
CPS = carbamoyl phosphate synthetase
FGARS = formylglycin ribonucleotide amidotransferase
ImGPS = imidazole glycerol phosphate synthase
PhzE = 2-amino-2-deoxyisochorismate synthase

Table 3.3: Oligonucleotides Used for Site-Directed Mutagenesis.

Mutant	**Primer-forward**	**Primer-reverse**
*st*TrpE_L2_D367A	CTGGCGCGCAATGACC	CGCGACCAGCATCAGATGTT
*st*TrpE_L2_D367E	TGGCGCGCAATGACCTG	GTTCGACCAGCATCAGATGT
*bl*PhzE_D250A	GAAGAACTGAAAATGATGGCACG	CGCCAGAACCATATACAGTTCG
*bl*PhzE_D250E	GAAGAACTGAAAATGATGGCAC	TTCCAGAACCATATACAGTTCG
*ec*PabB_D308A	CGTTAATGCGTAATGAT	CGACAATCATCAGATT
*ec*PabB_D308E	GAATTAATGCGTAATGATATCGGTCG	GACAATCATCAGATTTTCGGCAC
*tm*HisF_D98A	GCGAAGGTGAGCATAAACACGG	CGCACCACGGAGAAT
*tm*HisF_D98E	GAAAAGGTGAGCATAAACACGG	CGCACCACGGAGAAT

Table 3.4: Amino Acid Sequences of Analyzed Enzymes.

> *Burkholderia lata* 383 (*bl*) PhzE - Accession Number: WP_011355173

MNAAPNRNLFDRVLHGQAPCFALIARSTGSAGERAMIDVFAGAVSYPSSLAELPLAAPT
ATGADRQELLVMVPYRQLHERGFKTHDDGAPLVAITCDEHETVSAQLALAAIPDADTA
LGERHFDIDDEAYAEIVERVITDEIGTGAGSNFVIKRTLEGDLDDYSPAKALAVFKRLM
RREVGAYWIFVIHTGERTFVGATPERHLTLHEGCATMNPISGTYRYPQSGPTIDGINAF
LGDRKESDELYMVLDEELKMMARICPAGGQVTGPHLREMARLAHTEYFIVGHTEADV
RDLLRETMFAPTVTGSPIESATRVIARHERAGRGYYSGIAALIGRDARGGRTLDSAILIR
TAEIDRAGHVRIGVGSTLVRHSDAVSEVMETHAKVAALSNAFDPPEAGPALGQHPSVQ
AALRERNEGIADFWFRPYGGRQGEMADELAELSGCRALIVDAEDHFTAMIAQQLSSLG
LATEVCGVHDAVDLARYDVVVMGPGPGDPSDAGDPRIARLYAWLRHLIDEGKPFMAV
CLSHQILNAILGIPLVRREVPNQGIQVEIDLFGQRERVGFYNTYVAQTVRDEMDVDGVG
TVAISRDPRTGEVHALRGPTFSSMQFHAESVLTVDGPRILGEAITHAIRREKRMTALTA

> *Salmonella typhimurium* strain LT2 (*st*) TrpE -
Accession Number: WP_001194371

MQTPKPTLELLTCDAAYRENPTALFHQVCGDRPATLLLESADIDSKDDLKSLLLVDSAL
RITALGDTVTIQALSDNGASLLPLLDTALPAGVENDVLPAGRVLRFPPVSPLLDEDARLC
SLSVFDAFRLLQGVVNIPTQEREAMFFGGLFAYDLVAGFEALPHLEAGNNCPDYCFYL
AETLMVIDHQKKSTRIQASLFTASDREKQRLNARLAYLSQQLTQPAPPLPVTPVPDMRC
ECNQSDDAFGAVVRQLQKAIRAGEIFQVVPSRRFSLPCPSPLAAYYVLKKSNPSPYMFF
MQDNDFTLFGASPESSLKYDAASRQIEIYPIAGTRPRGRRADGTLDRDLDSRIELDMRT
DHKELSEHLMLVDLARNDLARICTPGSRYVADLTKVDRYSYVMHLVSRVVGELRHDLD
ALHAYRACMNMGTLSGAPKVRAMQLIADAEGQRRGSYGGAVGYFTAHGDLDTCIVIR
SALVENGIATVQAGAGIVLDSVPQSEADETRNKARAVLRAIATAHHAQETF

> *Salmonella typhimurium* strain LT2 (*st*) TrpG - Accession Number: ELN96503

MADILLLDNIDSFTWNLADQLRTNGHNVVIYRNHIPAQTLIDRLATMKNPVLMLSPGPG
VPSEAGCMPELLTRLRGKLPIIGICLGHQAIVEAYGGYVGQAGEILHGKASSIEHDGQAM
FAGLANPLPVARYHSLVGSNVPAGLTINAHFNGMVMAVRHDADRVCGFQFHPESILTT
QGARLLEQTLAWAQQK

> *Escherichia coli* K12 (*ec*) PabA- Accession Number: WP_000601847

MILLIDNYDSFTWNLYQYFCELGADVLVKRNDALTLADIDALKPQKIVISPGPCTPDEA
GISLDVIRHYAGRLPILGVCLGHQAMAQAFGGKVVRAAKVMHGKTSPITHNGEGVFRG
LANPLTVTRYHSLVVEPDSLPACFDVTAWSETREIMGIRHRQWDLEGVQFHPESILSEQ
GHQLLANFLHR

> *Escherichia coli* K12 (*ec*) PabB - Accession Number: WP_000854958

MKTLSPAVITLLWRQDAAEFYFSRLSHLPWAMLLHSGYADHPYSRFDIVVAEPICTLTT
FGKETVVSESEKRTTTTDDPLQVLQQVLDRADIRPTHNEDLPFQGGALGLFGYDLGRR
FESLPEIAEQDIVLPDMAVGIYDWALIVDHQRHTVSLLSHNDVNARRAWLESQQFSPQE
DFTLTSDWQSNMTREQYGEKFRQVQEYLHSGDCYQVNLAQRFHATYSGDEWQAFLQ
LNQANRAPFSAFLRLEQGAILSLSPERFILCDNSEIQTRPIKGTLPRLPDPQEDSKQAVKL
ANSAKDRAENLMIVDLMRNDIGRVAVAGSVKVPELFVVEPFPAVHHLVSTITAQLPEQL
HASDLLRAAFPGGSITGAPKVRAMEIIDELEPQRRNAWCGSIGYLSFCGNMDTSITIRTL
TAINGQIFCSAGGGIVADSQEEAEYQETFDKVNRILKQLEK

> *Thermotoga maritima* strain ATCC 43589 (*tm*) HisH -
Accession Number: WP_004080484.1

MRIGIISVGPGNIMNLYRGVKRASENFEDVSIELVESPRNDLYDLLFIPGVGHFGEGMRR
LRENDLIDFVRKHVEDERYVVGVCLGMQLLFEESEEAPGVKGLSLIEGNVVKLRSRRLP
HMGWNEVIFKDTFPNGYYYFVHTYRAVCEEEHVLGTTEYDGEIFPSAVRKGRILGFQF
HPEKSSKIGRKLLEKVIECSLSRR

> *Thermotoga maritima* strain ATCC 43589 (*tm*) HisF -
Accession Number: WP_004080486.1

MLAKRIIACLDVKDGRVVKGTNFENLRDSGDPVELGKFYSEIGIDELVFLDITASVEKRK
TMLELVEKVAEQIDIPFTVGGGIHDFETASELILRGADKVSINTAAVENPSLITQIAQTFG
SQAVVVAIDAKRVDGEFMVFTYSGKKNTGILLRDWVVEVEKRGAGEILLTSIDRDGTK
SGYDTEMIRFVRPLTTLPIIASGGAGKMEHFLEAFLAGADAALAASVFHFREIDVRELKE
YLKKHGVNVRLEGL

Chapter 4

Comprehensive Summary, Discussion, and Outlook

4.1 Comprehensive Summary

Within this thesis, the allosteric communication network of ADCS was investigated (chapter 2) and the insights gained from this analysis were transferred to other members of the class I GATase enzyme family (chapter 3). Based on these and previous findings described in the literature, a generalized hypothesis of allosteric coupling for the entire enzyme family was developed. Central to this hypothesis are three conformational changes that lead to an enhancement in glutaminase activity as a consequence of ligand binding to the synthase subunit: (i) the movement of conserved aspartate residues of the synthase subunits that are located at the synthase-glutaminase interface towards specific acceptor residues adjacent to the catalytic center of the glutaminase (Figure 3.3), (ii) the reorientation of residues that are involved in binding of the substrate glutamine and (iii) the reorientation of residues that form the oxyanion hole motif (Figure 2.6). It is worth noting that not all members of class I GATases seem to rely on all three coupling mechanisms. For a couple of members, no aspartate residues at the glutaminase-synthase interface were identified (chapter 3.3.1) and for one member, pyridoxal 5'-phosphate synthase (Pdx1:Pdx2), it was previously shown (Strohmeier et al., 2006) that the proper formation of the oxyanion hole upon complex formation was exclusively responsible for stimulation of glutaminase activity at its glutaminase subunit Pdx2 (Figure 4.1). More, detailed analyses of allosteric transitions in other members of class I GATases are thus needed to further decipher the mode of glutaminase activation for each individual member of this family. The three conformational changes described in this thesis could thereby serve as a blueprint for future, focused studies.

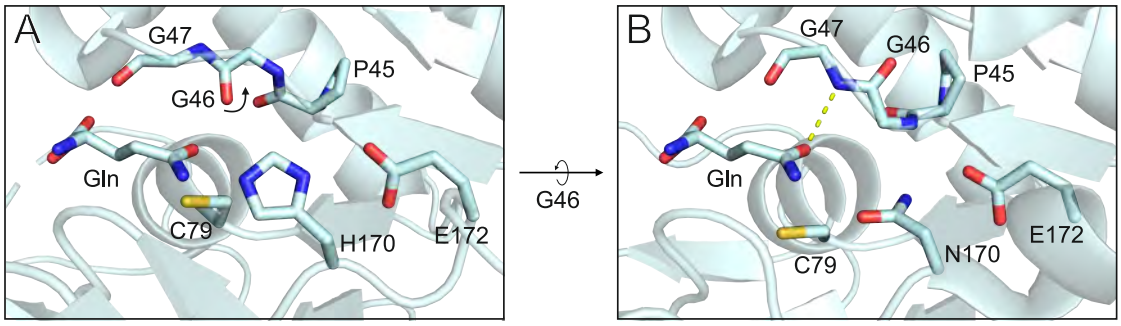

Figure 4.1: Oxyanion hole flip in pyridoxal 5'-phosphate synthase. (A) Uncomplexed Pdx2 glutaminase subunit (PDB ID: 2NV0). The oxyanion hole motif (P45-G46-G47) is in a catalysis incompetent conformation; specifically, the backbone amide of G47 is pointing away from the substrate glutamine. (B) Complexed Pdx1:Pdx2 (PDB ID: 2NV2). The backbone amide of G47 is presented to the carbonyl group of the glutamine to stabilize the oxyanion of the thioester-intermediates during catalysis. The stabilizing interaction between G47 and the carbonyl group of glutamine is indicated by yellow dashes. The complex structure of Pdx1:Pdx2 was solved with the Pdx2_H170N mutant.

4.2 Discussion: Reconciliation of the Postulated Activation Mechanisms with an Ensemble View of Allostery

The experimental data obtained for ADCS in the first part of this thesis were used to identify residues that are involved in a conformational transition that occurs in response to chorismate binding at the synthase subunit. The underlying assumption was that the functional states (active vs. inactive) are accurately represented by two well-defined structures (liganded vs. unliganded). While this classical *static view of allostery* was well suited to describe the significance of individual residues for allosteric activation, it was not adequate to interpret the allosteric deactivation observed for a significant number of alanine mutants of ADCS.

It is thus appropriate to reevaluate this classic allosteric model in light of novel findings in order to comprehensively interpret the obtained experimental data. Recent studies indicated that proteins more likely exist as a probabilistic distribution of energetically heterogeneous conformational states rather than just as two well-defined states (Motlagh et al., 2014). As a consequence, the *ensemble view of allostery* was developed. Thereby, the underlying assumption was that the active/inactive functional state are not adequately represented by two well-defined structures of a protein. In fact, even local unfolding and intrinsic protein disorder were shown to contribute to the conformational heterogeneity that ultimately allows for allosteric transitions (Motlagh et al., 2014). Congruously the *ensemble view of allostery* might be a more adequate model to describe allosteric transitions as it considers proteins as ensembles of different energetic states. For the enzymes studies here, the unliganded ensemble of states can thus be seen as an energetic distribution of inactive conformational states that each have a certain probability to accumulate. Ligand binding would then redistribute the conformational ensemble in a way that energetically favored (allosteric activation) or unfavored (allosteric deactivation) conformational states would accumulate (Figure 4.2).

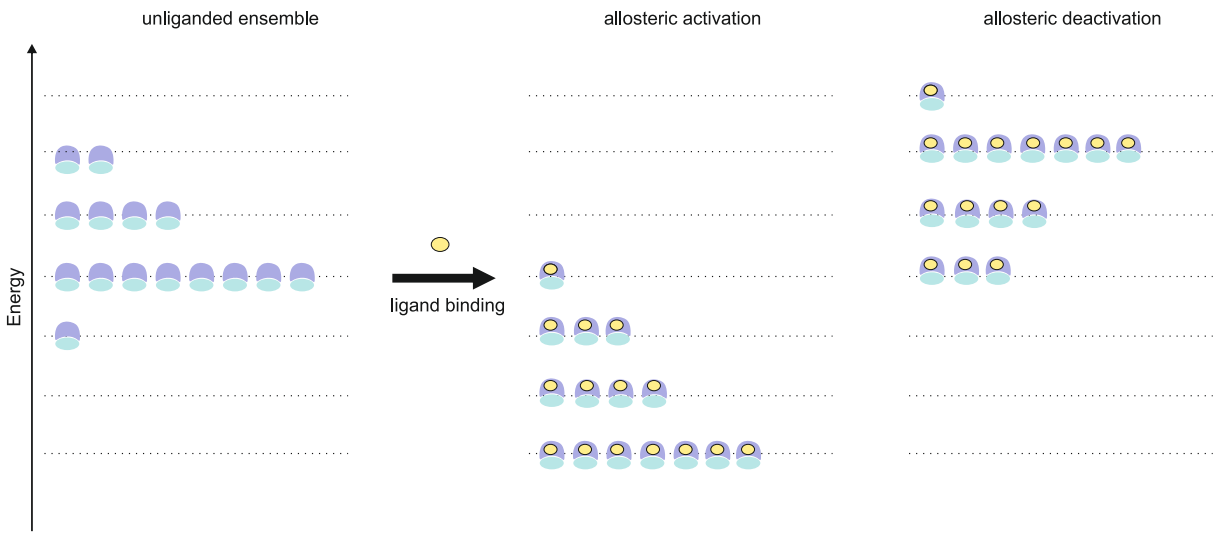

Figure 4.2: Ensemble view of allostery. In the unliganded ensemble, the different conformational states of a heterodimeric enzyme complex are distributed over a range of energetic levels energy (dashed, horizontal lines). Ligand binding redistributes the relative quantity of conformational states to different energetic levels. Allosteric activation redistributes the ensemble of conformational states to lower energetic levels and allosteric deactivation to higher energetic levels.

Experimental approaches to analyze ensemble states of allosteric proteins rely most heavily on solution NMR techniques (Velyvis et al., 2007; Tsai and Nussinov, 2014; Lisi and Loria, 2016). Thus, it is worth noting that PabA from *Escherichia coli* as well as the three ancestral PabA enzymes *anc*1-3PabA were not amenable for solution NMR techniques (unpublished data) and thus the *ensemble view of allostery* developed here solely relies on the presented data obtained by classical biochemical experiments.

4.3 Outlook: Antimicrobial Potential of Class I GATases Involved in Chorismate Metabolism

Over the last years, an alarming rise of antibiotic resistant infections has started to spread globally. These cumulated in the appearance of an *E. coli* strain carrying the mobilized colistin resistance-1 (mcr) gene that allows bacteria to resist the last resort antibiotics of the polymyxin group (Liu et al., 2016). Constant mutation and horizontal transfer of this gene to other bacteria has now resulted in a world-wide occurrence of strains harboring the mcr1-gene (Wang et al., 2018). According to recent data, the spread of antibiotic-resistant infections into the community is responsible for increased morbidity and mortality (Shore and Coukell, 2016). Without instant interference, the community might soon face a *post-antibiotic* era, in which even common infections could again cause life-threatening diseases. In addition to a more faithful use of antibiotics in human and animal therapies, society is thus in urgent need for novel, innovative antibiotics that target multi-drug resistant pathogens.

A promising but largely unexplored alternative mode of antibacterial action is the specific inhibition of essential bacterial protein-protein interactions (PPIs) (Cossar et al., 2018). PPI-inhibtion results in a reduced chance of resistance development, since two correlating mutations on both interaction partners would be necessary to overcome drug binding without compromising wild-type activity. Due to usually large and flat interfaces, PPIs were initially considered poor targets compared to the small and specific interactions at the active site of an enzyme. However, while interface geometries vary drastically, it is surprising that PPI modulators that are in clinical studies target PPIs at hot-spot residues within a small, defined binding area (Cossar et al., 2018). In order to develop efficient PPI-modulators, such hot-spot residues have first to be identified by crystal structure and mutational analysis. These requirements are fulfilled for the GATases ADCS, AS, and PhzE described in this thesis. The mutational screening combined with biophysical and biochemical analysis of the mutated GATase complexes revealed for ADCS a network of conserved interaction hot-spot amino-acid residues at the synthase-glutaminase interface that is also, at least in part, present in AS and PhzE (Figure 4.3 A). Strikingly, the interaction hot-spot residues of ADCS, AS, and PhzE are not limited to a few organisms. Phylogenetic analysis of a large set of bacterial sequences revealed that they are almost ubiquitous and conserved (Figure 3.3). They also occur in many pathogens, including those on the WHO priority list and the so-called ESKAPE organisms (*Enterococcus faecium*, *Staphylococcus aureus*, *Klebsiella pneumoniae*, *Acinetobacter baumannii*, *Pseudomonas aeruginosa*, *Enterobacter spp.*). Interfering with this interaction hot-spot area by a small molecule inhibitor might therefore offer a potential new strategy for the development of novel antibiotics (Figure 4.3 B).

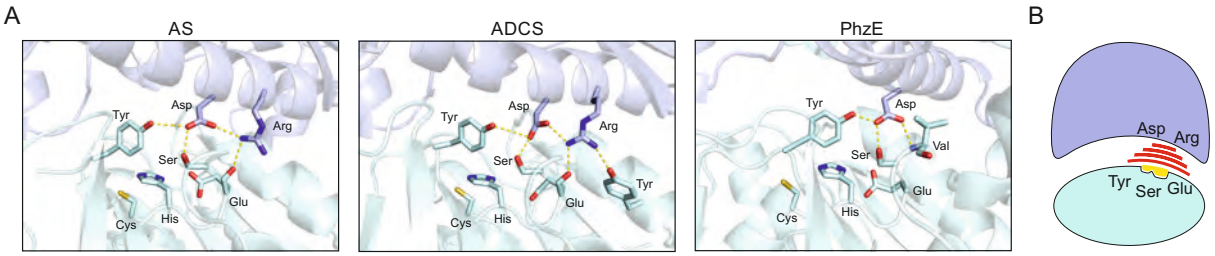

Figure 4.3: Interaction hot-spot residues in ADCS, AS, and PhzE. (A) Detailed structural view of the interfaces between synthase- and glutaminase subunits of ADCS, AS, and PhzE. The synthase subunit is depicted in blue, the glutaminase subunit in cyan. The catalytic triad (Cys-His-Glu) of the glutaminase subunit and interaction hot-spot residues are shown as sticks. Polar contacts are indicated by dashed, yellow lines. (B) Schematic representation of the GATase complex structure, the hot-spot amino acids at the interface, and the potential drug (yellow form) interference (red repulsion lines).

In order to evaluate GATases as potential targets for novel antibiotics, first experimental steps should focus on demonstrating that GATase enzyme inhibition of AS, ADCS, and PhzE by blockage of complex formation leads to bacteriostasis or conveys bactericidal effects. The *in vitro* assays described in this thesis would then be capable to screen commercially available fragment libraries to identify initial binding motifs that mimic the conserved interaction hot-spots of AS, ADCS, and PhzE. Our finding of clustered hot-spot residues in class I GATases might thus ultimately spur the antimicrobial potential of this fascinating family of enzymes.

References

Adams, P. D., R. W. Grosse-Kunstleve, L.-W. Hung, T. R. Ioerger, A. J. Mccoy, N. W. Moriarty, R. J. Read, J. C. Sacchettini, N. K. Sauter, and T. C. Terwilliger (2002). PHENIX: building new software for automated crystallographic structure determination. *Acta Crystallogr. D Biol. Crystallogr.*, 58(11):1948–1954.

Altschul, S. F., T. L. Madden, A. A. Schäffer, J. Zhang, Z. Zhang, W. Miller, and D. J. Lipman (1997). Gapped BLAST and PSI-BLAST: a new generation of protein database search programs. *Nucleic Acids Res.*, 25(17):3389–3402.

Amaro, R. E., A. Sethi, R. S. Myers, V. J. Davisson, and Z. A. Luthey-Schulten (2007). A network of conserved interactions regulates the allosteric signal in a glutamine amidotransferase. *Biochemistry*, 46(8):2156–2173.

Anand, R., A. A. Hoskins, J. Stubbe, and S. E. Ealick (2004). Domain organization of *Salmonella typhimurium* formylglycinamide ribonucleotide amidotransferase revealed by X-ray crystallography. *Biochemistry*, 43(32):10328–10342.

Bauer, J. A., E. M. Bennett, T. P. Begley, and S. E. Ealick (2004). Three-dimensional structure of YaaE from *Bacillus subtilis*, a glutaminase implicated in pyridoxal-5′-phosphate biosynthesis. *J. Biol. Chem.*, 279(4):2704–2711.

Beismann-Driemeyer, S. and R. Sterner (2001). Imidazole Glycerol Phosphate Synthase from *Thermotoga maritima*. *J. Biol. Chem.*, 276(23):20387–20396.

Bera, A. K., V. Atanasova, A. Dhanda, J. E. Ladner, and J. F. Parsons (2012). Structure of aminodeoxychorismate synthase from *Stenotrophomonas maltophilia*. *Biochemistry*, 51(51):10208–10217.

Bera, A. K., S. Chen, J. L. Smith, and H. Zalkin (1999). Interdomain signaling in glutamine phosphoribosylpyrophosphate amidotransferase. *J. Biol. Chem.*, 274(51):36498–36504.

Berendsen, H. J., D. Van Der Spoel, and R. Van Drunen (1995). GROMACS: a message-passing parallel molecular dynamics implementation. *Computer Phys. Comun.*, 91(1-3):43–56.

Binda, C., R. T. Bossi, S. Wakatsuki, S. Arzt, A. Coda, B. Curti, M. A. Vanoni, and A. Mattevi (2000). Cross-talk and ammonia channeling between active centers in the unexpected domain arrangement of glutamate synthase. *Structure*, 8(12):1299–1308.

Brannigan, J. A., G. Dodson, H. J. Duggleby, P. C. Moody, J. L. Smith, D. R. Tomchick, and A. G. Murzin (1995). A protein catalytic framework with an N-terminal nucleophile is capable of self-activation. *Nature*, 378(6555):416–419.

Bulloch, E. M., M. A. Jones, E. J. Parker, A. P. Osborne, E. Stephens, G. M. Davies, J. R. Coggins, and C. Abell (2004). Identification of 4-amino-4-deoxychorismate synthase as the molecular target for the antimicrobial action of (6S)-6-fluoroshikimate. *J. Am. Chem. Soc.*, 126(32):9912–9913.

Castresana, J. (2000). Selection of conserved blocks from multiple alignments for their use in phylogenetic analysis. *Mol. Biol. Evol.*, 17(4):540–552.

Chaudhuri, B. N., S. C. Lange, R. S. Myers, V. J. Davisson, and J. L. Smith (2003). Toward understanding the mechanism of the complex cyclization reaction catalyzed by imidazole glycerolphosphate synthase: crystal structures of a ternary complex and the free enzyme. *Biochemistry*, 42(23):7003–7012.

Chen, Y.-N. P., M. J. Lamarche, H. M. Chan, P. Fekkes, J. Garcia-Fortanet, M. G. Acker, B. Antonakos, C. H.-T. Chen, Z. Chen, and V. G. Cooke (2016). Allosteric inhibition of SHP2 phosphatase inhibits cancers driven by receptor tyrosine kinases. *Nature*, 535(7610):148–164.

Cossar, P. J., P. J. Lewis, and A. Mccluskey (2018). Protein-protein interactions as antibiotic targets: A medicinal chemistry perspective. *Med. Res. Rev.*, Pp. 1–26.

Crooks, G. E., G. Hon, J.-M. Chandonia, and S. E. Brenner (2004). WebLogo: a sequence logo generator. *Genome Res.*, 14(6):1188–1190.

Culbertson, J. E., D. H. Chung, K. T. Ziebart, E. Espiritu, and M. D. Toney (2015). Conversion of aminodeoxychorismate synthase into anthranilate synthase with Janus mutations: mechanism of pyruvate elimination catalyzed by chorismate enzymes. *Biochemistry*, 54(14):2372–2384.

Davies, G. M., K. J. Barrett-Bee, D. A. Jude, M. Lehan, W. W. Nichols, P. E. Pinder, J. L. Thain, W. J. Watkins, and R. G. Wilson (1994). (6S)-6-fluoroshikimic acid, an antibacterial agent acting on the aromatic biosynthetic pathway. *Antimicrob. Agents Chemother.*, 38(2):403–406.

Davis, I. W., A. Leaver-Fay, V. B. Chen, J. N. Block, G. J. Kapral, X. Wang, L. W. Murray, W. B. Arendall Iii, J. Snoeyink, and J. S. Richardson (2007). MolProbity: all-atom contacts and structure validation for proteins and nucleic acids. *Nucleic Acids Res.*, 35(suppl_2):W375–W383.

Douangamath, A., M. Walker, S. Beismann-Driemeyer, M. C. Vega-Fernandez, R. Sterner, and M. Wilmanns (2002). Structural evidence for ammonia tunneling across the $(\beta\alpha)_8$-barrel of the imidazole glycerol phosphate synthase bienzyme complex. *Structure*, 10(2):185–193.

Emsley, P. and K. Cowtan (2004). Coot: model-building tools for molecular graphics. *Acta Crystallogr. D Biol. Crystallogr.*, 60(12):2126–2132.

Fang, Z., C. Grütter, and D. Rauh (2012). Strategies for the selective regulation of kinases with allosteric modulators: exploiting exclusive structural features. *ACS Chem. Biol.*, 8(1):58–70.

Goto, M., R. Omi, N. Nakagawa, I. Miyahara, and K. Hirotsu (2004). Crystal structures of CTP synthetase reveal ATP, UTP, and glutamine binding sites. *Structure*, 12(8):1413–1423.

Gunasekaran, K., B. Ma, and R. Nussinov (2004). Is allostery an intrinsic property of all dynamic proteins? *Proteins: Struct. Funct. Bioinform.*, 57(3):433–443.

He, Z., K. D. Stigers Lavoie, P. A. Bartlett, and M. D. Toney (2004). Conservation of mechanism in three chorismate-utilizing enzymes. *J. Am. Chem. Soc.*, 126(8):2378–2385.

He, Z. and M. D. Toney (2006). Direct detection and kinetic analysis of covalent intermediate formation in the 4-amino-4-deoxychorismate synthase catalyzed reaction. *Biochemistry*, 45(15):5019–5028.

Hilser, V. (2010). An ensemble view of allostery. *Science*, 5966(327):653–654.

Holinski, A., K. Heyn, R. Merkl, and R. Sterner (2017). Combining ancestral sequence reconstruction with protein design to identify an interface hotspot in a key metabolic enzyme complex. *Proteins: Struct. Funct. Bioinform.*, 85(2):312–321.

Huang, X., H. M. Holden, and F. M. Raushel (2001). Channeling of substrates and intermediates in enzyme-catalyzed reactions. *Annu. Rev. Biochem.*, 70(1):149–180.

Kabsch, W. (1993). Automatic processing of rotation diffraction data from crystals of initially unknown symmetry and cell constants. *J. Appl. Crystallogr.*, 26(6):795–800.

Katoh, K. and D. M. Standley (2013). MAFFT multiple sequence alignment software version 7: improvements in performance and usability. *Mol. Biol. Evol.*, 30(4):772–780.

Kenakin, T. and L. J. Miller (2010). Seven transmembrane receptors as shapeshifting proteins: the impact of allosteric modulation and functional selectivity on new drug discovery. *Pharmacol. Rev.*, 62(2):265–304.

Kim, J. H., J. M. Krahn, D. R. Tomchick, J. L. Smith, and H. Zalkin (1996). Structure and function of the glutamine phosphoribosylpyrophosphate amidotransferase glutamine site and communication with the phosphoribosylpyrophosphate site. *J. Biol. Chem.*, 271(26):15549–15557.

Knöchel, T., A. Ivens, G. Hester, A. Gonzalez, R. Bauerle, M. Wilmanns, K. Kirschner, and J. N. Jansonius (1999). The crystal structure of anthranilate synthase from *Sulfolobus solfataricus*: functional implications. *Proc. Natl. Acad. Sci. U S A*, 96(17):9479–9484.

Koshland Jr, D., G. Nemethy, and D. Filmer (1966). Comparison of experimental binding data and theoretical models in proteins containing subunits. *Biochemistry*, 5(1):365–385.

Krieger, E. and G. Vriend (2014). YASARA View—molecular graphics for all devices—from smartphones to workstations. *Bioinformatics*, 30(20):2981–2982.

Lartillot, N., T. Lepage, and S. Blanquart (2009). PhyloBayes 3: a Bayesian software package for phylogenetic reconstruction and molecular dating. *Bioinformatics*, 25(17):2286–2288.

Li, Q.-A., D. V. Mavrodi, L. S. Thomashow, M. Roessle, and W. Blankenfeldt (2011). Ligand binding induces an ammonia channel in 2-amino-2-desoxyisochorismate (ADIC) synthase PhzE. *J. Biol. Chem.*, 286(20):18213–18221.

Lindahl, E., B. Hess, and D. Van Der Spoel (2001). GROMACS 3.0: a package for molecular simulation and trajectory analysis. *Mol. Model. Annu.*, 7(8):306–317.

Lipchock, J. M. and J. P. Loria (2010). Nanometer propagation of millisecond motions in V-type allostery. *Structure*, 18(12):1596–1607.

Lisi, G. P., A. A. Currier, and J. P. Loria (2018). Glutamine hydrolysis by imidazole glycerol phosphate synthase displays temperature dependent allosteric activation. *Front. Mol. Biosci.*, 5(4):1–12.

Lisi, G. P. and J. P. Loria (2016). Solution NMR spectroscopy for the study of enzyme allostery. *Chem. Rev.*, 116(11):6323–6369.

List, F., M. Bocola, M. C. Haeger, and R. Sterner (2012a). Constitutively active glutaminase variants provide insights into the activation mechanism of anthranilate synthase. *Biochemistry*, 51(13):2812–2818.

List, F., M. C. Vega, A. Razeto, M. C. Häger, R. Sterner, and M. Wilmanns (2012b). Catalysis uncoupling in a glutamine amidotransferase bienzyme by unblocking the glutaminase active site. *Chem. Biol.*, 19(12):1589–1599.

Liu, Y.-Y., Y. Wang, T. R. Walsh, L.-X. Yi, R. Zhang, J. Spencer, Y. Doi, G. Tian, B. Dong, and X. Huang (2016). Emergence of plasmid-mediated colistin resistance mechanism MCR-1 in animals and human beings in China: a microbiological and molecular biological study. *Lancet. Infect. Dis.*, 16(2):161–168.

Löytynoja, A. and N. Goldman (2008). Phylogeny-aware gap placement prevents errors in sequence alignment and evolutionary analysis. *Science*, 320(5883):1632–1635.

Mareya, S. M. and F. M. Raushel (1994). A molecular wedge for triggering the amidotransferase activity of carbamoyl phosphate synthetase. *Biochemistry*, 33(10):2945–2950.

Massiere, F. and M.-A. Badet-Denisot (1998). The mechanism of glutamine-dependent amidotransferases. *Cell. Mol. Life Sci.*, 54(3):205–222.

Mccoy, A. J., R. W. Grosse-Kunstleve, P. D. Adams, M. D. Winn, L. C. Storoni, and R. J. Read (2007). Phaser crystallographic software. *J. Appl. Crystallogr.*, 40(4):658–674.

Monaghan, D. T., M. W. Irvine, B. M. Costa, G. Fang, and D. E. Jane (2012). Pharmacological modulation of NMDA receptor activity and the advent of negative and positive allosteric modulators. *Neurochem. Int.*, 61(4):581–592.

Monod, J., J.-P. Changeux, and F. Jacob (1963). Allosteric proteins and cellular control systems. *J. Mol. Biol.*, 6(4):306–329.

Monod, J., J. Wyman, and J.-P. Changeux (1965). On the nature of allosteric transitions: a plausible model. *J. Mol. Biol.*, 12(1):88–118.

Morollo, A. A. and M. J. Eck (2001). Structure of the cooperative allosteric anthranilate synthase from *Salmonella typhimurium*. *Nat. Struct. Mol. Biol.*, 8(3):243–247.

Motlagh, H. N., J. O. Wrabl, J. Li, and V. J. Hilser (2014). The ensemble nature of allostery. *Nature*, 508(7496):331–339.

Mouilleron, S., M. A. Badet-Denisot, B. Badet, and B. Golinelli-Pimpaneau (2011). Dynamics of glucosamine-6-phosphate synthase catalysis. *Arch. Biochem. Biophys.*, 505(1):1–12.

Mouilleron, S. and B. Golinelli-Pimpaneau (2007). Conformational changes in ammonia-channeling glutamine amidotransferases. *Curr. Opin. Struct. Biol.*, 17(6):653–664.

Murshudov, G. N., A. A. Vagin, and E. J. Dodson (1997). Refinement of macromolecular structures by the maximum-likelihood method. *Acta Crystallogr. D Biol. Crystallogr.*, 53(3):240–255.

Myers, R. S., R. E. Amaro, Z. A. Luthey-Schulten, and V. J. Davisson (2005). Reaction coupling through interdomain contacts in imidazole glycerol phosphate synthase. *Biochemistry*, 44(36):11974–11985.

Nakatsu, T., H. Kato, and J. I. Oda (1998). Crystal structure of asparagine synthetase reveals a close evolutionary relationship to class II aminoacyl-tRNA synthetase. *Nat. Struct. Biol.*, 5(1):15–19.

Negre, C. F., U. N. Morzan, H. P. Hendrickson, R. Pal, G. P. Lisi, J. P. Loria, I. Rivalta, J. Ho, and V. S. Batista (2018). Eigenvector centrality for characterization of protein allosteric pathways. *Proc. Natl. Acad. Sci. U S A*, 115(52):E12201–E12208.

Oliver, J. C., R. Gudihal, J. W. Burgner, A. M. Pedley, A. T. Zwierko, V. J. Davisson, and R. S. Linger (2014). Conformational changes involving ammonia tunnel formation and allosteric control in GMP synthetase. *Arch. Biochem. Biophys.*, 545:22–32.

Ollis, D. L., E. Cheah, M. Cygler, B. Dijkstra, F. Frolow, S. M. Franken, M. Harel, S. J. Remington, I. Silman, J. Schrag, and E. Al. (1992). The alpha/beta hydrolase fold. *Prot. Eng.*, 5(3):197–211.

Parsons, J. F., P. Y. Jensen, A. S. Pachikara, A. J. Howard, E. Eisenstein, and J. E. Ladner (2002). Structure of *Escherichia coli* aminodeoxychorismate synthase: architectural conservation and diversity in chorismate-utilizing enzymes. *Biochemistry*, 41(7):2198–2208.

Perutz, M., M. Rossmann, A. Cullis, H. Muirhead, G. Will, and A. North (1960). Structure of hemoglobin. *Nature*, 185:416–422.

Plach, M. G., F. Semmelmann, F. Busch, M. Busch, L. Heizinger, V. H. Wysocki, R. Merkl, and R. Sterner (2017). Evolutionary diversification of protein–protein interactions by interface add-ons. *Proc. Natl. Acad. Sci. U S A*, 114(40):E8333–E8342.

Potterton, L., S. Mcnicholas, E. Krissinel, J. Gruber, K. Cowtan, P. Emsley, G. N. Murshudov, S. Cohen, A. Perrakis, and M. Noble (2004). Developments in the CCP4 molecular-graphics project. *Acta Crystallogr. D Biol. Crystallogr.*, 60(12):2288–2294.

Raschle, T., N. Amrhein, and T. B. Fitzpatrick (2005). On the two components of pyridoxal 5′-phosphate synthase from *Bacillus subtilis*. *J. Biol. Chem.*, 280(37):32291–32300.

Raushel, F. M., J. B. Thoden, and H. M. Holden (1999). The amidotransferase family of enzymes: molecular machines for the production and delivery of ammonia. *Biochemistry*, 38(25):7891–7899.

Raushel, F. M., J. B. Thoden, and H. M. Holden (2003). Enzymes with molecular tunnels. *Acc. Chem. Res.*, 36(7):539–548.

Rayl, E. A., J. M. Green, and B. P. Nichols (1996). *Escherichia coli* aminodeoxychorismate synthase: analysis of pabB mutations affecting catalysis and subunit association. *Biochim. Biophys. Acta*, 1295(1):81–88.

Rivalta, I., G. P. Lisi, N.-S. Snoeberger, G. Manley, J. P. Loria, and V. S. Batista (2016). Allosteric communication disrupted by a small molecule binding to the imidazole glycerol phosphate synthase protein–protein interface. *Biochemistry*, 55(47):6484–6494.

Rivalta, I., M. M. Sultan, N.-S. Lee, G. A. Manley, J. P. Loria, and V. S. Batista (2012). Allosteric pathways in imidazole glycerol phosphate synthase. *Proc. Natl. Acad. Sci. U S A*, 109(22):E1428–E1436.

Rohweder, B., F. Semmelmann, C. Endres, and R. Sterner (2018). Standardized cloning vectors for protein production and generation of large gene libraries in *Escherichia coli*. *BioTechniques*, 64(1):24–26.

Roux, B. and C. T. Walsh (1992). p-aminobenzoate synthesis in *Escherichia coli*: kinetic and mechanistic characterization of the amidotransferase PabA. *Biochemistry*, 31(30):6904–6910.

Roy, A., A. Kucukural, and Y. Zhang (2010). I-TASSER: a unified platform for automated protein structure and function prediction. *Nat. Protoc.*, 5(4):725–749.

Schadt, H. S., S. Schadt, F. Oldach, and R. D. Süssmuth (2009). 2-Amino-2-deoxyisochorismate is a key intermediate in *Bacillus subtilis* p-aminobenzoic acid biosynthesis. *J. Am. Chem. Soc.*, 131(10):3481–3483.

Schrödinger, L. (2018). The pymol molecular graphics system.

Selvy, P. E., R. R. Lavieri, C. W. Lindsley, and H. A. Brown (2011). Phospholipase D: enzymology, functionality, and chemical modulation. *Chem. Rev.*, 111(10):6064–6119.

Semmelmann, F., K. Straub, J. Nazet, C. Rajendran, R. Merkl, and R. Sterner (2019). Mapping the allosteric communication network of aminodeoxychorismate synthase. *J. Mol. Biol.*, 431(15):2718–2728.

Shore, C. K. and A. Coukell (2016). Roadmap for antibiotic discovery. *Nat. Microbiol.*, 1(6):16083.

Spraggon, G., C. Kim, X. Nguyen-Huu, M.-C. Yee, C. Yanofsky, and S. E. Mills (2001). The structures of anthranilate synthase of *Serratia marcescens* crystallized in the presence of (i) its substrates, chorismate and glutamine, and a product, glutamate, and (ii) its end-product inhibitor, L-tryptophan. *Proc. Natl. Acad. Sci. U S A*, 98(11):6021–6026.

Straub, K. and R. Merkl (2019). *Ancestral sequence reconstruction as a tool for the elucidation of a stepwise evolutionary adaptation*, Pp. 171–182. New York, NY: Humana Press.

Strohmeier, M., T. Raschle, J. Mazurkiewicz, K. Rippe, I. Sinning, T. B. Fitzpatrick, and I. Tews (2006). Structure of a bacterial pyridoxal 5′-phosphate synthase complex. *Proc. Natl. Acad. Sci. U S A*, 103(51):19284–19289.

Tesmer, J. J., T. J. Klem, M. L. Deras, V. J. Davisson, and J. L. Smith (1996). The crystal structure of GMP synthetase reveals a novel catalytic triad and is a structural paradigm for two enzyme families. *Nat. Struct. Biol.*, 3(1):74–86.

Thoden, J. B., H. M. Holden, G. Wesenberg, F. M. Raushel, and I. Rayment (1997). Structure of carbamoyl phosphate synthetase: a journey of 96 Å from substrate to product. *Biochemistry*, 36(21):6305–6316.

Thoden, J. B., X. Huang, F. M. Raushel, and H. M. Holden (1999). The small subunit of carbamoyl phosphate synthetase: snapshots along the reaction pathway. *Biochemistry*, 38(49):16158–16166.

Thoden, J. B., S. G. Miran, J. C. Phillips, A. J. Howard, F. M. Raushel, and H. M. Holden (1998). Carbamoyl phosphate synthetase: caught in the act of glutamine hydrolysis. *Biochemistry*, 37(25):8825–8831.

Tsai, C.-J. and R. Nussinov (2014). A unified view of "how allostery works". *PLoS Comp. Biol.*, 10(2):e1003394.

Velyvis, A., Y. R. Yang, H. K. Schachman, and L. E. Kay (2007). A solution NMR study showing that active site ligands and nucleotides directly perturb the allosteric equilibrium in aspartate transcarbamoylase. *Proc. Natl. Acad. Sci. U S A*, 104(21):8815–8820.

Viswanathan, V., J. M. Green, and B. P. Nichols (1995). Kinetic characterization of 4-amino 4-deoxychorismate synthase from *Escherichia coli*. *J. Bacteriol.*, 177(20):5918–5923.

Wang, R., L. Dorp, L. P. Shaw, P. Bradley, Q. Wang, X. Wang, L. Jin, Q. Zhang, Y. Liu, and A. Rieux (2018). The global distribution and spread of the mobilized colistin resistance gene mcr-1. *Nat. Commun.*, 9(1):1–9.

Wang, W. and B. A. Malcolm (1999). Two-stage PCR protocol allowing introduction of multiple mutations, deletions and insertions using QuikChange site-directed mutagenesis. *BioTechniques*, 26(4):680–682.

Waterhouse, A. M., J. B. Procter, D. M. Martin, M. Clamp, and G. J. Barton (2009). Jalview Version 2—a multiple sequence alignment editor and analysis workbench. *Bioinformatics*, 25(9):1189–1191.

Wheeler, L. C., S. A. Lim, S. Marqusee, and M. J. Harms (2016). The thermostability and specificity of ancient proteins. *Curr. Opin. Struct. Biol.*, 38:37–43.

Yang, J., R. Yan, A. Roy, D. Xu, J. Poisson, and Y. Zhang (2015). The I-TASSER Suite: protein structure and function prediction. *Nat. Methods*, 12(1):7–8.

Zalkin, H. and J. L. Smith (1998). Enzymes utilizing glutamine as an amide donor. *Adv. Enzymol. Relat. Areas Mol. Biol.*, 72:87–144.

Zein, F., Y. Zhang, Y.-N. Kang, K. Burns, T. P. Begley, and S. E. Ealick (2006). Structural insights into the mechanism of the PLP synthase holoenzyme from *Thermotoga maritima*. *Biochemistry*, 45(49):14609–14620.

Zhang, Y. and J. Skolnick (2005). TM-align: a protein structure alignment algorithm based on the TM-score. *Nucleic Acids Res.*, 33(7):2302–2309.

Acknowledgement

I want to thank Prof. Dr. Reinhard Sterner for his constant and generous support throughout this thesis. His unfettered, straightforward willingness to solve problems has inspired me to tap my full potential and he therefore had a big influence on my personal way of approaching new research questions. I want to cordially thank him for giving me the security and orientation I needed to succeed with this thesis. I also want to thank him for creating a work atmosphere that is built on trust and reliability which I have sensed as very enriching on the professional as well as on the personal level.

I want to thank Prof. Dr. Rainer Merkl for his genuine support, help and advice. He was a great mentor to this thesis and also a very inspiring person.

I would like to thank Prof. Dr. Johannes Buchner for mentoring this thesis and Prof. Dr. Remco Sprangers and his group for NMR support.

The collaborations with Prof. Dr. Joachim Ruther have been very instructive and fruitful. I want to cordially thank him for his genuine support.

All former and current members of the Institute of Biophysics and Physical Biochemistry helped create a very productive and encouraging work atmosphere. I thank you all for your advice, help, and the fun time we had.

I want to gratefully acknowledge financing and the opportunity to participate in a variety of highly interesting seminars & trainings by the *Konrad-Adenauer-Stiftung*.

I want to thank Ann-Kathrin Baier, Sophia Dlugos, Regina Hertle, Cosimo Kropp, Zora Machacek, Benedikt Moissl, and Alisa Ruisinger for their commitment during their research internships or Master's theses. Each of you contributed valuable puzzle pieces to this thesis and I am thankful for the time we had.

My heartfelt thank goes out to Sabine Laberer, Sonja Fuchs, Christiane Endres, Ulrike Stökl, and Jeanette Ueckert. The impact your unrestricted technical help had on the success of this thesis can hardly be put into words.

My parents, my brother and my grand-parents have always been my greatest supporters and words hardly do justice to express the gratitude I feel for everything you enabled me to do. I want to thank Emanuel, Marilena, Andrea, Thomas, Natalie, and Jesse for being the most awesome, reliable, and lovely friends one could possibly imagine. Angela, you are my sunshine and I want to thank you for your love.